Responses to the comments on the paper by Referees

Referee's comments are in *blue italic*, our comments are in black, manuscript's changes are in red.

Response to the comments on the paper by Referee #1

Major Points:

1. *There are a number of problems in the way the MLS data are presented and used. First, it is not clear that the day-night differences are being used for the "standard" HO2 product, as recommended in validation papers and in MLS data quality documents. This is critical since HO2 is a major focus for the paper. Second, there is no mention of the version of the data used (v3.3?) and whether all of the appropriate data screens were used. Third, all of the figures show data and profiles to 0.01 hPa, when in fact the useful range for HO2 is clearly stated at 0.046 hPa, and for O3 at 0.02 hPa. Data above these levels are not recommended for science purposes and should not be part of the analysis. This paper would clearly benefit from some interaction and discussion with members of the MLS team to ensure that the data are being applied correctly.*

We agree with this comment. In the revised manuscript the following corrections are made (see lines 322-333):

(1) We have used the day-minus-night differences for the HO_2 product. Accordingly, the results presented in Figs. 2–6 have been completely recalculated.

(2) The information on the MLS data version in use, i.e. v4.2, the latest one, have been added. All the data screens were applied when dealing with the MLS standard product.

(3) We have limited our analysis to the 1–0.046 mbar pressure interval where all data are suitable for scientific use, as prescribed by (Wang et al., 2015; Livesey et. al., 2017).

2. The connection between the CTM results and the analytic formulation is not sufficiently explored. Figure 1 is used to show that the difference between the CTM and equilibrium equation is a few percent or less, and that this justifies the use of the analytic formulation in the subsequent statistical evaluation. However, there is not enough information given about the CTM to judge whether or not this is really an independent validation. Presumably, the CTM uses the same set of reactions and the same equilibrium assumptions along with the "family" chemical species approach, so it is not surprising that

they agree. It is also not clear whether the CTM also includes NOx chemistry, which might have an impact in the upper stratosphere and lower mesosphere.

We agree that the original version of the manuscript contained little information about the 3D chemical transport model (CTM). Indeed, our model uses a family concept by Shimazaki (Shimazaki, 1985). It is used to calculate the evolution of the components of HOx and NOx families, while the Ox family is calculated via regular implicit Euler method. Moreover, it should be emphasized that the Shimazaki scheme utilizes an implicit Euler scheme too and does not use the steady state approximation for short-lived components. Thus, in calculating the evolution of OH, HO_2, and O_3 within the framework of the CTM, we *do not use* the photochemical equilibrium condition.

In the revised manuscript the following changes have been made:

(1) A list of reactions, accounted for by the CTM, is added (see Table 1). It can be seen first of all, that the CTM includes comprehensive NOx chemistry. Secondly, the complete set of reactions (63 in total) is much bigger than the one we consider to describe the daytime balance of OH, HO_2, and O_3 concentrations. In the original manuscript there were 9 of them — now there are 8, the reaction $OH + HO_2 \rightarrow H_2O + O_2$ was removed. Our numerical analysis showed that its contribution to the analytic expression $F(OH, HO_2, O_3) = 1$ is less than 1%.

(2) The description of the chemical transport model, including its dynamics and the integration methods used, is substantially expanded (see lines 167-195). In particular, it is stated that «The evolution of the components of HO_x (H, OH, HO_2, H_2O_2) and NO_x (N, NO, NO_2, NO_3) families is calculated using the chemical family concept proposed by Shimazaki (Shimazaki, 1985). This is done because of the presence of short-lived components among these families, with lifetimes much shorter than those of the families themselves, which imposes significant restrictions on the value of the CTM's integration step. For example, the daytime lifetimes of OH and HO_2 above 70 km are about 1 s or less, while the lifetime of the HO_x family is about 10^4 s or more. Therefore, when calculating these components individually it is necessary to set the CTM's integration step to be much less than 1 s. In our work, the Shimazaki technique is applied for calculating the evolution of each component of the HO_x and NO_x families. We emphasize that this technique does not explicitly use the steady-state approximation for the components, instead it utilizes the approach based on an implicit Euler scheme (see Shimazaki, 1985). This allows increasing the integration step of CTM significantly without loss of accuracy of calculating the short-lived components. In our work the integration time is chosen to be 9 s.»

As a further example, there are known effects on HOx and NOx in the mesosphere from energetic particle precipitation events [e.g. many papers by Jackman et al and Verronen et al], and it would be important for the CTM to include these if it is intended to be used as a validation of the equilibrium expression. In fact, Figures 2 and 3 display data from January 2005, during a period with a documented SPE event [Jackman etal., ACP, 2011]. The possible influence of SPE perturbations needs to be discussed and addressed.

Done. We carried out a brief analysis of the possible effect of solar proton events (SPE), which were not implemented in the CTM, on the mesospheric photochemistry in daytime. We considered the most prominent impact of SPE in the context of the problem: the impact on the chemical balance of OH. Comparing the additional OH source due to SPE with the main source of this component (via the reactions $HO_2 + O \rightarrow OH + O_2$, $H + O_3 \rightarrow OH + O_2$ and $H + HO_2 \rightarrow 2OH$) we showed that the influence of SPE on the daytime balance of OH is insignificant.

We made two additions to the revised manuscript:

(1) a new figure (see Fig. 2);

(2) the following text (see lines 251-256, 263-275):

«Note also that Eq. (1) and Eq. (6) take into account only the main daytime source of OH (P_{OH}) specified by reactions R18, R14, and R21:

$$P_{OH}=k_{18}\cdot HO_2\cdot O+2k_{14}\cdot HO_2\cdot H+k_{21}\cdot O_3\cdot H$$

These reactions run “inside” the HOx (H, OH, HO_2, H_2O_2) family and do not perturb its total concentration. The height–latitude cross-sections of $<P_{OH}>$ for each month are presented in Fig. 2.

….

Another source of OH is sporadically activated during charged particle precipitation events and exists for a relatively short time (several days). Solar proton events (SPE) perturb the ionic composition in the mesosphere and the upper stratosphere considerably and trigger a whole cascade of reactions involving ions, neutral components and their clusters (e.g., $O_2^+\cdot H_2O$). This leads to an additional (to reactions R59 and R7) conversion of H_2O molecules into OH and H (Solomon et al., 1981). The maximum of the OH production rate (P_{OH}^{SPE}) induced by SPE is located in the polar latitudes in the region of 60–80 km and, as a rule, does not exceed $2\cdot10^3$ cm^{-3} s^{-1} (Jackman et al., 2011, 2014). It can be seen from Fig. 2 that at these latitudes and altitudes the P_{OH}^{SPE}/P_{OH} ratio does not exceed 1-2%, even for the maximum values of P_{OH}^{SPE}. This means that the impact of P_{OH}^{SPE} on Eq. (6) is of the same order of smallness as in the case of reactions R59 and R7, hence, it may be

neglected. A similar conclusion can be made for other reactions from Table 1, not accounted for by Eq. (6), including the ones involving NO_x in both quiet and perturbed conditions in the mesosphere.»

(3) We found the mistake in Fig. 1 below 50 km caused by the use of improper computer number format (float32 instead of float64). So Fig.1 was recalculated and redrawn. The value of $< F >$ below 50 km increases.

If the CTM includes a comprehensive simulation of all known reactions and processes impacting HOx, and there is still agreement with the analytic approach, then the results are more credible. The paper should demonstrate that in fact the CTM provides a complete description of HOx photochemistry.

Done. To sum up, the following corrections have been made:

(1) A list of reactions is added, accounted for by the CTM. It can be seen that the CTM includes complete chemistry of the mesosphere.

(2) The description of the chemical transport model is substantially expanded in the part relating to dynamics and the methods of integration applied.

(3) Analysis of the possible effect of solar proton events (SPE), which are not implemented in our model, on the photochemistry in the daytime mesosphere is carried out.

Finally, there is a problem with converting pressure altitudes in the model to pressures by assuming a constant scale height of 7 km. This assumption can lead to offsets of 1 km or larger and is particularly critical when comparing vertical profiles with large gradients. For example, at 62 km the US std atmosphere has a pressure of 0.1671 mb. If a constant 7-km scale height is used in the expression in the paper, one would calculate p=0.1442 at 62 km. The analysis in this paper should use the temperatures in the model to compute convert altitude to pressure using hydrostatic equilibrium on a layer-by-layer basis.

Done. In the revised manuscript, the pseudo-height scale was replaced by pressure levels (see lines 199-202 and Figs 1-3). In addition, we indicated the approximate heights in km which were calculated for a given month utilizing averaged temperature profiles of the model and hydrostatic equilibrium.

3. There is not enough detail on the conclusion that the offline HO2 product better agrees with the statistical retrieval. First, there is no direct comparison between the offline product and the statistical retrieval, as there is for the standard product and the statistical retrieval (figs 4-6). There is only a presentation of the offline HO2 product, and the reader has to

refer back to figs 4-6 and then estimate just how much better the agreement really is. The improvement needs to be quantified more directly. Also, there is no discussion as to why the agreement is better and this really gets down to the science. Does this paper intend to suggest that the offline HO2 product is superior to the standard product? If so, then the discussion/conclusion needs to be expanded to clearly justify why this is so. There also needs to be some explanation for why the offline product is different in the first place, without forcing to reader to go back and review the Milan et al [2015] paper.

Done. First of all, the description of the offline HO_2 retrieval is expanded and its advantages over the standard MLS product are pointed out (see lines 395-403):

«Moreover, new data on the HO_2 distributions were recently obtained from the MLS measurements. Millán et al. (2015) performed the offline retrieval of daily zonal means of HO_2 profiles using averaged MLS radiances measured in 10° latitude bins. Averaged spectra have a better signal to noise ratio, which removes many of the limitations of the MLS standard product for HO_2. In particular, the upper boundary of the altitude region in which daytime data is suitable for scientific use has reached 0.0032 mbar, and the "day-minus-night" correction is not needed at altitudes above 1 mbar. Comparison with various experimental and model data has shown that the offline retrieval reproduces the basic properties of the HO_2 distribution in the mesosphere relatively well (at least qualitatively) (Millán et al. 2015).»

Second, we made a direct comparison (see Fig. 10) of the offline MLS product with the results of our statistical retrieval and the standard product of MLS. One can see from Fig. 10 that our results better match the offline product than the standard one. The most noticeable difference is in the location of the mesospheric maximum of the HO_2 concentration. According to the standard product it is close to 0.1 mbar, while the retrieved data and the offline product demonstrate the altitudes above 0.046 mbar. This is also confirmed by the HO_2 distributions calculated using our 3D chemical transport model (see lines 391-394 and Fig. 9), In the revision we highlighted (see lines) that the higher location of that maximum in the results of the of HO_2 statistical retrieval is due to the influence of MLS data on OH, which have the mesospheric maximum (see Figs. 6–8) also well above 0.1 mbar.

Minor Points:

The grammar and wording is awkward or incorrect in a number of places, for example Abstract: "statistically correct approach" is not illuminating. One would not expect ACP to publish a "statistically incorrect approach". Suggest a "Bayesian statistical approach".

Corrected. "statistically correct approach" was replaced by "statistical approach" everywhere in text. See lines 14, 135.

"air concentration" is more generally "neutral density",

Corrected. "air concentration" was replaced by "neutral density" everywhere in text. See lines 19, 141.

"air temperature" is generally just "temperature".

Corrected. "air temperature" was replaced by "temperature" everywhere in text. See lines 19, 141, 323.

*"We have performed *a* one-year simulation".*

Corrected. See line 20.

Last sentence is unclear. Also "MLS primary data", what is primary data? Perhaps this should be MLS radiances.

Corrected. See lines 29-30.

In terms of the reaction sets, there appears to be a gaping omission of the HOx production reactions, H2O+hv and H2O+O(1D). These should be included for completeness; however, I suspect their terms may drop out when forming the ratio OH/HO2.

Done. We have directly compared the source of OH ($P_{OH}^{H_2O}$) due to the reactions $H_2O+h\nu \rightarrow H+OH$ and $O(^1D)+H_2O \rightarrow 2OH$ with the main source of that component, P_{OH}, via the reactions $HO_2 + O \rightarrow OH + O_2$, $H + O_3 \rightarrow OH + O_2$ and $H + HO_2 \rightarrow 2OH$. The ratio $P_{OH}^{H_2O} / P_{OH}$ does not exceed 3-4%.

Two corrections are made in the revised manuscript:

(1) new figures are added (Fig. 2-3);

(2) the following text is inserted (lines 251-262):

«Note also that Eq. (1) and Eq. (6) take into account only the main daytime source of OH (P_{OH}) specified by reactions R18, R14, and R21:

$$P_{OH}=k_{18} \cdot HO_2 \cdot O + 2k_{14} \cdot HO_2 \cdot H + k_{21} \cdot O_3 \cdot H$$

These reactions run “inside” the HOx (H, OH, HO_2, H_2O_2) family and do not perturb its total concentration. The height–latitude cross-sections of $<P_{OH}>$ for each month are presented in Fig. 2.

The next important daytime source of OH is specified by reactions R59 and R7 involving H_2O, the main source for the HO_x family:

$$P_{OH}^{H_2O}=(k_{59}+2\cdot k_7\cdot O(^1D))\cdot H_2O$$

Figure 3 shows height–latitude cross-sections of $<P_{OH}^{H_2O}/P_{OH}>$ for each month. Comparing Fig. 1 and Fig. 3, we conclude that the previously indicated 3–4 % deviation of $<F>$ from 1 in the region between 76 km and 86 km is largely due to the neglect of these reactions.»

When deriving equation 14, which forms a major basis for the paper, I was not able to reproduce the authors' results and cannot comment on the validity of this result. It seems much more complicated than the text would suggest. I strongly recommend an appendix which details the step-by-step process at arriving at equation 14.

The whole section (Sec.2) was rewritten at the price of an insignificant increase in volume. Including, all the steps needed to derive the equation $F(OH,HO_2,O_3)=1$ are presented. We believe that in this form this section harmoniously fits into the main canvas.

Figure 3 is unclear what ranges of latitudes are being shown.

Corrected. See Fig. 5.

Figs 4-6 contain horizontal dotted lines but these are not explained in the text or caption.

This horizontal dotted lines marked the upper limit of air pressure (0.046 mbar) where HO_2 data are suitable for scientific use. In the revised manuscript we restricted the pressure range by 0.046 mbar.

Response to the comments on the paper by Referee #2

Main text:

On the one hand the authors use model results of 3D-calculations and on the other hand they employ measured concentrations of these species. Deviations from unity are a hint to non-equilibrium conditions or to other reasons such as incorrect reaction rates, erroneous model calculations or errors in the retrieved data. The fundamental idea was to derive such expression not depending on water vapor. The interpretation of deviations from unity is certainly complicated. What means for instance -1% deviation or F(OH, HO_2, O_3)=0.99? It indicates that, generally speaking, the agreement is quite good. But in case of stronger deviations it is difficult to say, what is the reason for this discrepancy?

In the revised manuscript (see Fig. 3 and lines 251-262), we have directly compared the source of OH ($P_{OH}^{H_2O}$) due to the reactions $H_2O+h\nu \rightarrow H+OH$ и $O(^1D)+H_2O \rightarrow 2OH$ with the main source of that component, P_{OH}, via the reactions $HO_2 + O \rightarrow OH + O_2$, $H + O_3 \rightarrow OH + O_2$ and $H + HO_2 \rightarrow 2OH$. It can be seen from Fig. 1 and Fig. 3 that the indicated 3–4 % deviation of $<F>$ from 1 in the region between 76 km and 86 km is largely due to the neglect of the reactions $H_2O+h\nu \rightarrow H+OH$ и $O(^1D)+H_2O \rightarrow 2OH$.

Also, one should note the following. We found the mistake in Fig. 1 below 50 km caused by the use of improper computer number format (float32 instead of float64). The value of $<F>$ below 50 km increases.

Minor comments:

The paper has a very voluminous introduction of about 39% related to the entire paper. It has the character of a review paper. I will it not criticize that, but I will it only mention here.

Indeed, the Introduction contains elements of the review. Thus, we wanted to show that the proposed method of evaluation of simultaneous measurements of mesospheric components has a wide range of possible applications for other areas of the atmosphere.

Line 165: 150 km is already the middle thermosphere.

Corrected. See line 166.

Line 174: entered, maybe better mentioned

Corrected. See line 197.

Line 178: H=7 km is an approximated mean scale height. (1 km scale height corresponds to about 33 K or 7 km to 231 K mean temperature)

Corrected (see lines 197-202 and Figs 1-3). In the revised manuscript, the pseudo-height scale was replaced by pressure levels. In addition, we indicated the approximate heights in km calculated from the pressure profiles for a given month utilizing averaged temperature profiles of the model and hydrostatic equilibrium.

Line 194: reaction rate constants; according to? Quotation?

Corrected. See line 227 and Table 1.

Line 198: The net production term of hydrogen radicals is in essential JH2O[H2O]. Why do you neglect this term in (10)? Too small compared with the other terms in equation (10) and consequently the approach do not depend on water vapor?

In the revised manuscript, we have directly compared the source of OH ($P_{OH}^{H_2O}$) due to the reactions $H_2O+h\nu \rightarrow H+OH$ and $O(^1D)+H_2O \rightarrow 2OH$ with the main source of that component, P_{OH}, via the reactions $HO_2 + O \rightarrow OH + O_2$, $H + O_3 \rightarrow OH + O_2$ and $H + HO_2 \rightarrow 2OH$. The ratio $P_{OH}^{H_2O} / P_{OH}$ does not exceed 3-4%.

Two corrections are made in the revised manuscript:

(1) a new figure is added (Fig. 2-3);

(2) the following text is inserted (lines 251-262):

«Note also that Eq. (1) and Eq. (6) take into account only the main daytime source of OH (P_{OH}) specified by reactions R18, R14, and R21:

$$P_{OH}=k_{18}\cdot HO_2\cdot O+2k_{14}\cdot HO_2\cdot H+k_{21}\cdot O_3\cdot H$$

These reactions run “inside” the HOx (H, OH, HO_2, H_2O_2) family and do not perturb its total concentration. The height–latitude cross-sections of $<P_{OH}>$ for each month are presented in Fig. 2.

The next important daytime source of OH is specified by reactions R59 and R7 involving H_2O, the main source for the HO_x family:

$$P_{OH}^{H_2O}=(k_{59}+2\cdot k_7\cdot O(^1D))\cdot H_2O$$

Figure 3 shows height–latitude cross-sections of $<P_{OH}^{H_2O} / P_{OH}>$ for each month. Comparing Fig. 1 and Fig. 3, we conclude that the previously indicated 3–4 % deviation of

$< F >$ from 1 in the region between 76 km and 86 km is largely due to the neglect of these reactions.»

Line 202: ...of ozone ()?

Corrected. See line 230.

Line 204: The aim is to eliminate O and H and to derive an expression only depending on OH, HO2, O3.

Done. We added new sentence (see line 228):

«We eliminate O and H from Eqs. (1)-(3) and derive an expression depending only on OH, HO_2, O_3.»

Line 211: α=(...) could be equation (14.2) and (14) then (14.1) or (15) and the following equations (x+1). There is a large step from equation (10) – (13) to equation (14). Could you give some intermediate steps?

Done. The Sec.2 was rewritten. All the steps needed to derive the equation $F(OH, HO_2, O_3) = 1$ were presented. It should be noted that the reaction OH + $HO_2 \rightarrow H_2O$ + O_2 was removed from the analysis. Our numerical calculations showed that its contribution to the analytic expression $F(OH, HO_2, O_3) = 1$ is less than 1%.

Line 218: k2 decreases strongly below the lower mesosphere and stratopause. Ozone is no longer in photochemical equilibrium there.

We cannot fully agree with the comment. In particular, daytime lifetime of O_3 in the altitude range of 30-50 km varies in the range 100-1000 s (Brasseur and Solomon, 2005). So, O_3 can stay in photochemical equilibrium depending on height and duration of daylight.

The following sentences were inserted in the revised manuscript (see lines 247-250):

„Note that these components remain short-lived below 50 km (with the lifetimes of about 10^2-10^3 s (Brasseur and Solomon, 2005)) depending on height and duration of daylight. However, for quantitative description of their daytime equilibrium it is necessary to include additional reactions involving, in particular, the components of the NO_x family."

Line 234:...certain altitude z...

Corrected. See line 290.

Line: 239: Factor σj√2π?

Corrected. See line 295.

Line 296:...fall into one...

Corrected. See line 360.

Line 304-318: In the lower thermosphere the system is not in chemical equilibrium. Transports play a significant role (see also Grygalashvyly et al. 2012).

Section 6: The characteristic time of atomic oxygen is about $\tau O=(k1*O_2*M)^{-1}$ *. At 90km is* $O_2=1.47x10^{13}$ cm^{-3}, $M=7x10^{13}$ cm^{-3}, *and* $k1\approx10^{-33}$ cm^6s^{-1} *depending on temperature. The characteristic time has then an order of* 10^6 *s. About one order smaller is the characteristic time of H, but still large. Both the production and the loss term of* HO_2 *depend on H and O being not in photochemical equilibrium in the lower thermosphere. Therefore a discrepancy relating to HO2 one should expect.*

Here, apparently, there was a misunderstanding caused by a possibly insufficiently clear indication in the manuscript. In these parts (Lines 304-318 (new 368-383), Section 6) we consider lower and middle mesosphere, heights below 0.01 mbar (~78km). In the revised manuscript, the upper height is 0.046 mbar (~71-72 km).

Technical Note: Evaluation of simultaneous measurements of mesospheric OH, HO_2, and O_3 under photochemical equilibrium assumption: Statistical approach

Mikhail Yu. Kulikov[1], Anton A. Nechaev[1], Mikhail V. Belikovich[1], Tatiana S. Ermakova[1], and Alexander M. Feigin[1]

[1]Institute of Applied Physics of the Russian Academy of Sciences, 46 Ulyanov Str., 603950 Nizhny Novgorod, Russia

Correspondence to: Mikhail Yu. Kulikov (mikhail_kulikov@mail.ru)

Abstract

The Technical Note presents a ~~statistically correct~~ statistical approach to evaluating simultaneous measurements of several atmospheric components under the assumption of photochemical equilibrium. We consider simultaneous measurements of OH, HO_2, and O_3 at the altitudes of the mesosphere as a specific example and their daytime photochemical equilibrium as an evaluating relationship. A simplified algebraic equation relating local concentrations of these components in the 50-100 km altitude range has been derived. The parameters of the equation are ~~air~~ temperature, ~~air concentration~~ neutral density, local zenith angle, and the rates of ~~9~~ 8 reactions. We have performed a one-year simulation of the mesosphere and lower thermosphere using a 3D chemical-transport model. The simulation shows that the discrepancy between the calculated evolution of the components and the equilibrium value given by the equation does not exceed 3-4% in the full range of altitudes independent of season or latitude. We have developed the technique of statistic Bayesian evaluation of simultaneous measurements of OH, HO_2 and O_3 based on the equilibrium equation taking into account the measurement error. The first results of application of the technique to MLS/Aura data are presented in this Technical Note. It has been found that the satellite data of HO_2 distribution regularly demonstrates essentially lower altitudes of mesospheric maximum of this component. This has also been confirmed by model HO_2 distributions and comparison with offline retrieval of HO_2 from the daily zonal means MLS ~~primary data~~ radiance.

1. Introduction

A prominent feature of the atmospheric photochemical systems is the presence of a large number of chemical components with short lifetime and concentrations close to stable photochemical equilibrium at every instant. The condition of balance between their sources and sinks is described by a system of algebraic equations. This system can be used to determine characteristics of hard to measure atmospheric species through other measurable components, validate results of remote or *in situ* measurements, estimate reaction rates usually known with significant uncertainty, and to understand processes and chemical reactions that influence variability of the most important atmospheric components, e.g. ozone, in the geographical region of interest.

This approach has found wide application:

(1) in 3D chemical transport models that include a large set of physical and chemical processes with a broad spectrum of spatio-temporal scales. In particular, the chemical family concept is widely used for simulating gas phase photochemistry of the lower and middle atmosphere (e.g., Douglass et al., 1989; Kaye and Rood, 1989; Rasch et al., 1995), when transport is taken into account only for the concentration of a chemical family, while relative concentrations of the constituent fast components are calculated from the instantaneous stable equilibrium condition. Complemented with the Henry law (e.g., Djouad et al., 2003; Tulet et al., 2006) in multiphase models, this approach markedly saves calculation time and increases the overall stability of the numerical scheme. Moreover, the use of the photochemical equilibrium condition to simulate fast components dynamics reduces the phase space dimension of box models significantly (e.g., Kulikov and Feigin, 2014), allowing a comprehensive analysis of nontrivial nonlinear dynamic properties of various atmospheric photochemical systems (e.g., Feigin and Konovalov, 1996; Feigin et al., 1998; Konovalov et al., 1999; Konovalov and Feigin, 2000; Kulikov et al., 2012).

(2) in investigations of the chemistry of the surface layer and free troposphere in different regions (over megalopolises, in rural areas, in the mountains, over the seas) based on measurements of nitrogen species, peroxy radicals, ozone, aerosols, and other components aimed at understanding processes impacting the surface ozone formation and air quality. The equilibrium condition is most frequently used for nitrogen species. For example, Chameides (1975) proposed a model for determining the vertical distribution of odd nitrogen, in which the HNO_3 profile could be

deployed to retrieve profiles of five other components (NO, NO_2, NO_3, N_2O_5, and HNO_2) from their photochemical equilibrium condition. In the paper by Stedman et al. (1975) the equation for NO_2 equilibrium that accounted only for the main source and sink of this component was applied to determine the photodissociation constant $J(NO_2)$. A more accurate equation for the NO_2 equilibrium was used by Crawford et al. (1996) and Kondo et al. (1996) to determine the NO_2/NO partitioning and NO_x, allowing, in particular, investigating the spatial distribution of NO_x/NO_y over the Pacific.

Night-time equilibrium in the NO_2-NO_3-N_2O_5 system is used to determine surface layer N_2O_5 concentration, equilibrium constant of this system, equilibrium partitioning between NO_3 and N_2O_5, and loss coefficients of NO_3, N_2O_5 and NO_x (Martinez et al., 2000; Brown et al., 2003; Crowley et al., 2010; McLaren et al., 2010; Benton et al., 2010; Sobanski et al., 2016).

Platt et al. (1979) used the CH_2O photochemical equilibrium condition to analyse results of simultaneous measurement of CH_2O, O_3 and NO_2 and to identify mechanisms of CH_2O formation over rural areas and in maritime air. In the papers by Ko et al. (2003), Cantrell et al. (2003), Penkett et al. (1997), Penkett et al. (1998) algebraic expressions derived from equilibrium conditions for H_2O_2, peroxy radicals and nitrogen species were used to determine equilibrium values of peroxide concentration, total peroxy radical level, and NO/NO_2 ratio, and to diagnose the ozone production and loss levels in clean or polluted troposphere.

(3) in stratospheric chemistry studies, including determination of a critical parameter in catalytic cycles of ozone destruction in the polar stratosphere. In particular, the equilibrium condition for ClO and Cl_2O_2 along with the measurement data of daytime and night-time concentrations of these components in the polar stratosphere are used to evaluate the temperature dependence of the ClO concentration, reaction constants determining the $ClO + ClO + M \leftrightarrow Cl_2O_2 + M$ equilibrium, and the photolysis rate of Cl_2O_2 (Ghosh et al., 1997; Avallone et al., 2001, Solomon et al., 2002; Stimpfle et al., 2004; von Hobe et al., 2005; Berthet et al., 2005; Butz et al., 2007; von Hobe et al., 2007; Kremser et al., 2011; Sumińska-Ebersoldt et al., 2012; Wetzel et al., 2012).

Pyle et al. (1983) proposed a method for derivation of the OH concentration from satellite infrared measurements of NO_2 and HNO_3 using a simple algebraic relation following from the equilibrium condition for HNO_3. Algorithms for retrieving distributions of OH and HO2 from the satellite measurement data of O_3, NO_2, H_2O, HNO_3 by LIMS/Nimbus 7 and UARS with the help of algebraic models following from the photochemical equilibrium of O_x, HO_x and HNO_3 components

were proposed by Pyle and Zavody (1985), Pickett and Peterson (1996). It is also worthy of note that similar models are widely used for calculating concentrations of components with a short lifetime (e.g. $O(^1D)$ and OH) and subsequent evaluating vertical distributions of eddy diffusivity from measurements of trace gas concentration profiles (see, e.g., Massie and Hunten, 1981).

Kondo et al. (1988) made use of the photochemical equilibrium between NO and NO_2 for understanding diurnal variations of NO concentration measured during aircraft flights. In the paper by Webster et al. (1990) simultaneous *in situ* balloon-borne measurements of NO, NO_2, HNO_3, O_3 and N_2O and the photochemical equilibrium condition for various nitrogen components were used to determine OH, N_2O_5 and NO_y concentrations. A similar approach was employed by Kawa et al. (1990), who obtained NO_2, N_2O_5, $ClNO_3$, HNO_3 and OH concentrations from aircraft measurements of NO, ClO and O_3 concentrations. Hauchecorne et al. (2010) found that NO_3 concentration measured by GOMOS/ENVISAT positively correlates with temperature at altitudes up to 45 km in the region where NO_3 is in chemical equilibrium with O_3. Funke et al. (2005) used NO and NO_2 stable-state photochemistry to verify correctness of the new approach of retrieving distributions of those component from MIPAS/ENVISAT measurement data. Marchland et al. (2007) proposed a method to retrieve the temperature distribution in the stratosphere between 30 km and 40 km from O_3 and NO_3 measurements by GOMOS with the help of a simple equation derived from the night-time NO_3 chemical equilibrium.

(4) in investigations of the chemistry of O_x–HO_x components and atmospheric glows in the mesosphere and MLT area. In particular, Kulikov et al. (2006, 2009) proposed algorithms for the simultaneous retrieval of O, H, HO_2 and H_2O from joint OH and O_3 satellite measurement, in which the assumption of photochemical equilibrium of O_3, OH, and HO_2 was utilized. For several decades the assumption of the photochemical equilibrium of ozone (PEO) was widely used to determine distributions of atomic oxygen and atomic hydrogen at altitudes of the MLT via satellite and rocket measurement of ozone concentration and airglow emissions (e.g., Evans and Llewellyn, 1973; Good, 1976; Pendleton et al., 1983; McDade et al., 1985; McDade and Llewellyn, 1988; Evans et al., 1988; Thomas, 1990; Llewellyn et al., 1993; Llewellyn and McDade, 1996; Mlynczak et al., 2007, 2013a, 2013b, 2014; Smith et al., 2010; Siskind et al., 2008, 2015). Russell and Lowe (2003) applied PEO to infer the seasonal and global climatology of atomic oxygen using WINDII/UARS. PEO was deployed to investigate hydroxyl emission mechanisms, morphology, and variability in the upper mesosphere – lower thermosphere region (Marsh et al., 2006; Xu et al., 2010, 2012;

Kowalewski et al., 2014). Mlynczak and Solomon (1991, 1993) and Mlynczak et al. (2013b) used the equilibrium assumption to derive exothermic chemical heat. The PEO assumption employed for studying the mesospheric OH* layer response to gravity waves (Swenson and Gardner, 1998). In ultimately theoretical works, e.g. Grygalashvyly et al. (2014), Grygalashvyly (2015), PEO was used to derive the dependence of excited hydroxyl layer concentration and altitude on atomic oxygen and temperature. In the paper by Sonnemann et al. (2015) it was used to analyze annual variations of OH* layer. Moreover, PEO is frequently applied implicitly, when authors are equating the night-time loss of ozone in the reaction with atomic hydrogen and production of ozone by a 3-body reaction of molecular and atomic oxygen (e.g., Nikoukar et al., 2007).

In the present Technical note we demonstrate how the photochemical equilibrium condition of several atmospheric components may be employed to statistically ~~correctly~~ validate data of their simultaneous measurements, particularly in the case when measurement error is large.

We consider the simultaneous photochemical daytime equilibrium of OH, HO_2, and O_3 at the altitudes of the mesosphere. We have derived a simplified algebraic equation

$$F(OH, HO_2, O_3) = 1,$$

describing the relationship between local concentrations of the components at the altitudes of 50–100 km. The only parameters of the equation are ~~air~~ temperature, ~~air concentration~~ neutral density, local zenith angle, and constants of ~~9~~ 8 reactions. One-year simulation of the mesosphere and lower thermosphere based on a 3D chemical-transport model shows that the discrepancy between the calculated evolution of the components and the equilibrium value given by the equation does not exceed 3–4 % in the full range of altitudes independent of season or latitude.

We have developed a technique of statistical Bayesian evaluation of simultaneous measurement of OH, HO_2 and O_3 based on the mentioned equilibrium equation taking into account the measurement error. The first results of its application to MLS/Aura data (Wang et al., 2015a,b; Schwartz et al., 2015) are presented. It is found that the satellite data of HO_2 distribution regularly demonstrates essentially lower altitudes of this component's mesospheric maximum. These results confirm the ones obtained via the offline retrieval of HO_2 from the MLS primary data (Millán et al., 2015).

The Technical Note is structured as follows. A 3D chemical transport model is briefly described in Sect. 2. In Sect. 3 a simplified algebraic relationship between the equilibrium concentrations of OH, HO_2 and O_3 is derived and verified by 3D simulations. Section 4 presents the

method of statistical evaluation of simultaneous data of OH, HO_2 and O_3. The results of applying the method to MLS/Aura data are presented in Sect. 5. The last Section contains discussion of the results followed by concluding remarks.

2. Model and calculations

For our calculations we used the global 3D chemical transport model (CTM) of the middle atmosphere developed by the Leibniz Institute of Atmospheric Physics (IAP) (e.g., Sonnemann et al., 1998). It was designed particularly for investigation of the spatio-temporal structure of phenomena in the MLT region and specifically in the extended mesopause region. ~~The model includes 3D advective and vertical diffusive transport (turbulent and molecular).~~ The grid-point model extends from the ground up to the ~~lower~~ middle thermosphere (0–150 km; 118 pressure-height levels). The horizontal resolution amounts to 5.625° latitudinally and 5.625° longitudinally. ~~The chemistry module consists of 19 constituents, 49 chemical reactions, and 14 photo-dissociation reactions. CTM was described in numerous papers (e.g., Sonnemann et al., 1998; Körner and Sonnemann, 2001; Grygalashvyly et al., 2009, 2011, 2012). It was validated, particularly for ozone, with measurement in a number of papers (Hartogh et al., 2004, 2011; Sonnemann et al., 2006a, 2006b, 2007). Three-dimensional fields of temperature and winds are used from the Canadian Middle Atmosphere Model (CMAM) for the year 2000 (de Grandpre et al., 2000; Scinocca et al., 2008).~~

The chemical module described in numerous papers (e.g., Sonnemann et al., 1998; Körner and Sonnemann, 2001; Grygalashvyly et al., 2009, 2011, 2012) consists of 19 constituents, 49 chemical reactions, and 14 photo-dissociation reactions (see Table 1). The reaction rates used in the model are taken from Burkholder et al. (2015). The temperature-dependent reaction rates are calculated on-line, thus, they are sensitive to small temperature fluctuations. We make use of the pre-calculated dissociation rates (Kremp et al., 1999).

The evolution of the components of HO_x (H, OH, HO_2, H_2O_2) and NO_x (N, NO, NO_2, NO_3) families is calculated using the chemical family concept proposed by Shimazaki (Shimazaki, 1985). This is done because of the presence of short-lived components among these families, with lifetimes much shorter than those of the families themselves, which imposes significant restrictions on the value of the CTM's integration step. For example, the daytime lifetimes of OH and HO_2

above 70 km are about 1 s or less, while the lifetime of the HO_x family is about 10^4 s or more. Therefore, when calculating these components individually it is necessary to set the CTM's integration step to be much less than 1 s. In our work, the Shimazaki technique is applied for calculating the evolution of each component of the HO_x and NO_x families. We emphasize that this technique does not explicitly use the steady-state approximation for the components, instead it utilizes the approach based on an implicit Euler scheme (see Shimazaki, 1985). This allows increasing the integration step of CTM significantly without loss of accuracy of calculating the short-lived components. In our work the integration time is chosen to be 9 s.

The model includes 3D advective and vertical diffusive transport (turbulent and molecular). Three-dimensional fields of temperature and winds are taken from the Canadian Middle Atmosphere Model (CMAM) for the year 2000 (de Grandpre et al., 2000; Scinocca et al., 2008). We use the Walcek-scheme (Walcek and Aleksic, 1998; Walcek, 2000) for advective transport and the implicit Thomas algorithm as described in Morton and Mayers (1994) for diffusive transport. The vertical eddy diffusion coefficient is based on the results by Lübken (1997).

The CTM driven by COMMA-IAP middle atmosphere dynamics (Berger, 1994; Ebel et al., 1995; Kremp et al., 1999; Berger and von Zahn, 1999) was verified by measurements, particularly for ozone, in a number of papers (Hartogh et al., 2004, 2011; Sonnemann et al., 2006, 2007).

We ~~calculated~~ calculate the annual variation of spatio-temporal distributions of OH, HO_2, and O_3 and constructed distributions of the $F(OH, HO_2, O_3)$ function introduced in Sect. 1. To remove transitional regions that correspond to sunset and sunrise, we ~~took~~ take into account only periods of local time with the solar zenith angle $\chi < 85°$. ~~The previous research based on satellite measurements had often showed results on pressure heights, or "pseudo altitudes". Following them, in the present paper we present our results on the pressure heights $z^* = -H \ln(p / p_0)$, where $H = 7$ km is the scale height, p is the pressure, and $p_0 = 1013$ hPa is the pressure at the surface.~~ The obtained results are presented in the model coordinates, so the pressure-height levels are used for the vertical axes. In addition, the approximate altitudes are shown in the figures of Sec. 1, calculated for a given month utilizing averaged temperature profiles of the model and hydrostatic equilibrium.

3. Daytime photochemical equilibrium of OH, HO_2, and O_3 at the altitudes of the mesosphere

~~The daytime balance of OH, HO_2, and O_3 concentrations at mesospheric altitudes is determined by the following primary reactions:~~

~~$O(^3P) + O_2 + M \rightarrow O_3 + M$, | k_1 (1)~~

~~$O_3 + h\nu \rightarrow O_2 + O(^1D, ^3P)$, | $k_2 = J_{O3} = J_1 + J_2$ (2)~~

~~$O_3 + H \rightarrow O_2 + OH$, | k_3 (3)~~

~~$O + OH \rightarrow O_2 + H$, | k_4 (4)~~

~~$O + HO_2 \rightarrow O_2 + OH$, | k_5 (5)~~

~~$O_2 + H + M \rightarrow HO_2 + M$, | k_6 (6)~~

~~$O_3 + OH \rightarrow O_2 + HO_2$, | k_7 (7)~~

~~$H + HO_2 \rightarrow 2OH$ | k_8 (8)~~

~~$OH + HO_2 \rightarrow H_2O + O_2$ | k_9 (9)~~

~~where k_1–k_9 are the corresponding reaction constants, J_{O3} is the total dissociation rate of ozone, which is the sum of two branches, J_1 and J_2, and M is air concentration.~~

The daytime balance of OH concentration at mesospheric altitudes is determined by the following primary reactions (Brasseur and Solomon, 2005):

$HO_2 + O \rightarrow OH + O_2$ (R18 in Table 1)

$H + O_3 \rightarrow OH + O_2$ (R21)

$H + HO_2 \rightarrow 2OH$ (R14)

$OH + O \rightarrow H + O_2$ (R17)

$OH + O_3 \rightarrow HO_2 + O_2$ (R22)

The daytime balance of HO_2 concentration:

$H + O_2 + M \rightarrow HO_2 + M$, M is molecule of air (R20)

$OH + O_3 \rightarrow HO_2 + O_2$ (R22)

$HO_2 + O \rightarrow O_2 + OH$ (R18)

The daytime balance of O_3 concentration:

$O + O_2 + M \rightarrow O_3 + M$ (R12)

$O_3 + h\nu \rightarrow O_2 + O$ (R52)

$O_3 + h\nu \rightarrow O_2 + O(^1D)$ (R53)

$O_3 + H \rightarrow OH + O_2$ (R21)

Expressions for local concentrations of OH, HO_2, and O_3 in the photochemical equilibrium are written in the form

~~$$OH = \left(k_3 \cdot O_3 \cdot H + k_5 \cdot HO_2 \cdot O + 2k_8 \cdot HO_2 \cdot H\right) / \left(k_4 \cdot O + k_7 \cdot O_3 + k_9 \cdot HO_2\right) \quad (10)$$~~

~~$$HO_2 = \left(k_6 \cdot M \cdot O_2 \cdot H + k_7 \cdot O_3 \cdot OH\right) / \left(k_5 \cdot O + k_8 \cdot H + k_9 \cdot OH\right) \quad (11)$$~~

~~$$O_3 = \frac{k_1 \cdot M \cdot O_2 \cdot O}{k_2 + k_3 \cdot H + k_7 \cdot OH} \quad (12)$$~~

$$OH = \frac{k_{18} \cdot HO_2 \cdot O + 2k_{14} \cdot HO_2 \cdot H + k_{21} \cdot O_3 \cdot H}{k_{17} \cdot O + k_{22} \cdot O_3}, \quad (1)$$

$$HO_2 = \frac{k_{20} \cdot M \cdot O_2 \cdot H + k_{22} \cdot O_3 \cdot OH}{k_{18} \cdot O}, \quad (2)$$

$$O_3 = \frac{k_{12} \cdot M \cdot O_2 \cdot O}{k_{52} + k_{53} + k_{21} \cdot H}, \quad (3)$$

where k_i are the corresponding reaction constants from Burkholder et al. (2015).

We eliminate O and H from Eqs. (1)-(3) and derive an expression depending only on OH, HO_2, O_3.

Almost everywhere in the mesosphere and lower thermosphere (with the exception of 85-95 km, see Kulikov et al., 2017) the photodissociation ~~reaction Eq. (2)~~ is the main ozone sink, i.e. ~~$k_2 >> k_3 \cdot H + k_7 \cdot OH$.~~ $k_{52} + k_{53} >> k_{21} \cdot H$. Therefore, in the zero order approximation Eq. (~~12~~ 3) can be simplified and the concentration of atomic oxygen can be defined in terms of ozone concentration:

~~$$O = \frac{k_2 \cdot O_3}{k_1 \cdot M \cdot O_2} \quad (13)$$~~

$$O = \frac{k_{52} + k_{53}}{k_{12} \cdot M \cdot O_2} O_3 \quad (4)$$

Making use of Eq. (~~13~~ 4) we can derive from Eq. (~~11~~ 2) an expression for the concentration of H in terms of concentrations of OH, HO_2 and O_3~~.~~ :

$$H = \frac{k_{18} \cdot (k_{52} + k_{53}) / (k_{12} \cdot M \cdot O_2) \cdot HO_2 - k_{22} \cdot OH}{k_{20} \cdot M \cdot O_2} O_3 \quad (5)$$

By substituting this equation and Eq. (~~13~~4) into Eq. (~~10~~1) we obtain an expression relating OH, HO_2, and O_3:

~~$F(OH,HO_2,O_3) = \alpha \cdot \frac{k_4 \cdot OH}{k_5 \cdot HO_2} = 1,$~~ ~~(14)~~

~~where~~

~~$\alpha = (1 + \frac{(k_7 + k_9 \cdot HO_2 / O_3) \cdot k_6 \cdot k_1 \cdot M \cdot O_2 + k_1 \cdot k_3 \cdot k_7 \cdot O_3 + 2 \cdot k_1 \cdot k_7 \cdot k_8 \cdot HO_2}{k_4 \cdot k_6 \cdot k_2}) / (1 + \frac{k_3 \cdot O_3 + 2 \cdot k_8 \cdot HO_2}{k_6 \cdot M \cdot O_2}).$~~

$$F(OH,HO_2,O_3) = \left(\frac{k_{20} \cdot M \cdot O_2}{k_{20} \cdot M \cdot O_2 + k_{21} \cdot O_3 + 2 \cdot k_{14} \cdot HO_2} + \frac{k_{12} \cdot M \cdot O_2 \cdot k_{22}}{(k_{52} + k_{53}) \cdot k_{17}}\right) \cdot \frac{k_{17} \cdot OH}{k_{18} \cdot HO_2} = 1 \quad (6)$$

Figure 1 shows height–latitude cross-sections of $<F(OH,HO_2,O_3)>$ for each month (in this Section angle brackets denote monthly averaged zonal mean values). The dashed area corresponds to χ > 85°. One can see that eq. (~~14~~ 15) is most accurate within the 50–~~80~~ 76 km range and above ~~90~~ 86 km, where $|<F> - 1| \le 1\%$. The difference reaches 3–4 % in the region between ~~80~~ 76 km and ~~90~~ 86 km. The altitude of this region has an annual variation with a maximum deviation in the winter hemisphere. Below 50 km the value of $<F>$ ~~sharply drops down~~ increases up to ~~0.25–0.30~~ 1.2 at 40 km ~~(not shown in Fig. 1),~~ thus below the stratopause Eq. (~~14~~ 6) no longer describes the simultaneous photochemical equilibrium of OH, HO_2 and O_3. Note that these components remain short-lived below 50 km (with the lifetimes of about 10^2-10^3 s (Brasseur and Solomon, 2005)) depending on height and duration of daylight. However, for quantitative description of their daytime equilibrium it is necessary to include additional reactions involving, in particular, the components of the NO_x family.

Note also that Eq. (1) and Eq. (6) take into account only the main daytime source of OH (P_{OH}) specified by reactions R18, R14, and R21:

$$P_{OH} = k_{18} \cdot HO_2 \cdot O + 2k_{14} \cdot HO_2 \cdot H + k_{21} \cdot O_3 \cdot H$$

These reactions run "inside" the HOx (H, OH, HO_2, H_2O_2) family and do not perturb its total concentration. The height–latitude cross-sections of $<P_{OH}>$ for each month are presented in Fig. 2.

The next important daytime source of OH is specified by reactions R59 and R7 involving H_2O, the main source for the HO_x family:

$$P_{OH}^{H_2O} = (k_{59} + 2 \cdot k_7 \cdot O(^1D)) \cdot H_2O$$

Figure 3 shows height–latitude cross-sections of $< P_{OH}^{H_2O} / P_{OH} >$ for each month. Comparing Fig. 1 and Fig. 3, we conclude that the previously indicated 3–4 % deviation of $< F >$ from 1 in the region between 76 km and 86 km is largely due to the neglect of these reactions.

Another source of OH is sporadically activated during charged particle precipitation events and exists for a relatively short time (several days). Solar proton events (SPE) perturb the ionic composition in the mesosphere and the upper stratosphere considerably and trigger a whole cascade of reactions involving ions, neutral components and their clusters (e.g., $O_2^+ \cdot H_2O$). This leads to an additional (to reactions R59 and R7) conversion of H_2O molecules into OH and H (Solomon et al., 1981). The maximum of the OH production rate (P_{OH}^{SPE}) induced by SPE is located in the polar latitudes in the region of 60–80 km and, as a rule, does not exceed $2 \cdot 10^3$ cm^{-3} s^{-1} (Jackman et al., 2011, 2014). It can be seen from Fig. 2 that at these latitudes and altitudes the P_{OH}^{SPE} / P_{OH} ratio does not exceed 1-2%, even for the maximum values of P_{OH}^{SPE}. This means that the impact of P_{OH}^{SPE} on Eq. (6) is of the same order of smallness as in the case of reactions R59 and R7, hence, it may be neglected. A similar conclusion can be made for other reactions from Table 1, not accounted for by Eq. (6), including the ones involving NO_x in both quiet and perturbed conditions in the mesosphere.

4. Method of statistical evaluation of simultaneous measurement of OH, HO_2 and O_3

The proposed method is based on the statistical Bayesian procedure described in the works by Kulikov et al. (2009) and Nechaev et al. (2016). It was originally developed for retrieving trace gas concentrations in the mesosphere from ground-based and satellite measurements of other mesospheric components. With respect to the considered evaluation problem this procedure consists of three steps: (1) constructing conditional probability density function (PDF) of OH, HO_2 and O_3 concentration values at each altitude z in the selected interval assuming that there is certain measurement data of these components and the algebraic relationship (~~14~~ 6) is valid; (2) calculating the first moments of this distribution, i.e. expected value and dispersion of each component using the Metropolis-Hastings algorithm (Chib and Greenberg, 1995) for multidimensional integration; (3) comparing the obtained results with the initial measurement data.

For constructing posterior PDF it is convenient to introduce vector ~~$\vec{u}\{HO_2^r, O_3^r, OH^r\}$~~ $\vec{u}\{HO_2^{ret}, O_3^{ret}, OH^{ret}\}$, whose components are the retrieved values of chemical species concentrations at a certain altitude z, and vector $\vec{x}\{HO_2^m, O_3^m, OH^m\}$ composed of experimentally measured values of the components of vector $\vec{u}$, $x_j = u_j + \xi_j$, $j = 1..3$, where ξ_j is a random error of measuring the j-th component of vector $\vec{u}$ at the altitude z. It is assumed that

(1) random variables ξ_j are distributed normally with densities

~~$$w_j(\xi_j) = \frac{1}{\sqrt{2\pi}\sigma_j} exp\left(\frac{\xi_j^2}{2\sigma_j^2}\right);$$~~ ~~(15)~~

$$w_j(\xi_j) = \frac{1}{\sigma_j\sqrt{2\pi}} exp\left(-\frac{\xi_j^2}{2\sigma_j^2}\right);$$ (7)

(2) ξ_j are mutually independent:

$$\vec{\xi}\{\xi_1, \xi_2, \xi_3\} \sim W_\xi(\vec{\xi}) = \prod_j w_j(\xi_j),$$ (~~16~~ 8)

where $W_\xi(\vec{\xi})$ is the total PDF of all ξ_j;

(3) dispersions σ_j in Eq. (~~15~~7), that are expected error values, are assumed to be known a priori (in our case they are provided by the MLS retrieval algorithm along with measured data).

Then the probability to observe vector $\vec{x}$ is given by the conditional PDF

$$P_x(\vec{x} \mid \vec{u}) = \int \delta(\vec{x} - \vec{u}) W_\xi(\vec{\xi}') d^3\vec{\xi}' = W_\xi(\vec{x} - \vec{u}),$$ (~~17~~ 9)

where $\delta(\ldots)$ is delta function.

The prior relationship of ~~HO_2^r~~ HO_2^{ret}, ~~O_3^r~~ O_3^{ret} and ~~OH^r~~ OH^{ret} concentrations (Eq. (~~14~~ 6)) can be written as $u_3 = G(u_1, u_2)$. Integrating the left-hand side of Eq. (17) with conditional PDF of the variable u_3:

$$P_{u_3}(u_3 \mid u_1, u_2) = \delta(u_3 - G(u_1, u_2)),$$

yields a likelihood function of the model

$$P_x(\vec{x} \mid u_1, u_2) = w_3(x_3 - G(u_1, u_2)) \cdot w_1(x_1 - u_1) w_2(x_2 - u_2).$$ (~~18~~ 10)

According to Bayes' theorem, the posterior function, i.e. the probability density of latent variables u_1

and u_2, under the condition that $\vec{x}$ is observed, is defined by the expression

$$P(u_1,u_2 \mid \vec{x}) \propto P_x(\vec{x} \mid u_1,u_2) \cdot P_{apr}(u_1,u_2)$$

$$\propto exp\left(-\frac{(x_1-u_1)^2}{2\sigma_1^2}\right) \cdot exp\left(-\frac{(x_2-u_2)^2}{2\sigma_2^2}\right) \cdot exp\left(-\frac{(x_3-G(u_1,u_2))^2}{2\sigma_3^2}\right) \cdot P_{apr}(u_1,u_2) \quad (\text{~~19~~ 11})$$

in which $P_{apr}(u_1,u_2)$ defines prior PDF of u_1 and u_2.

The retrieved value of the latent variable $u_{1,2,3}$ is hereinafter understood as the mean value of the function in Eq. (~~19~~ 11):

$$\langle u_{1,2} \rangle = \int_{-\infty}^{\infty} \int_{-\infty}^{\infty} u_{1,2} \cdot P(u_1,u_2 \mid \vec{x}) du_1 du_2$$

$$\langle u_3 \rangle = \int_{-\infty}^{\infty} \int_{-\infty}^{\infty} G(u_1,u_2) \cdot P(u_1,u_2 \mid \vec{x}) du_1 du_2. \quad (\text{~~20~~ 12})$$

Its dispersion defines the uncertainty of the retrieval:

$$\sigma_{u_j} = \sqrt{\langle u_j^2 \rangle - \langle u_j \rangle^2}, \quad j = 1..3, \quad (\text{~~21~~ 13})$$

where the angle brackets denote averaging in the sense of Eq. (~~20~~ 12).

5. MLS/Aura data evaluation and results

~~We used the results of simultaneous measurement of trace gas concentrations and air temperature $T^{MLS}(p)$ obtained with MLS/ Aura (Wang et al., 2015a,b; Schwartz et al., 2015) within the 10^0 – 10^{-2} hPa air pressure interval.~~ We used the latest version (v4.2) of the MLS "standard" product (Livesey et al., 2017) for trace gas concentrations and temperature T within the 1 – 0.046 mbar pressure interval where all data are suitable for scientific applications (Wang et al., 2015a,b; Schwartz et al., 2015). We took the daytime data when the solar zenith angle $\chi < 80°$ for January, May, and September 2005. All data were appropriately screened. "Pressure", "estimated precision", "status flag", "quality", "convergence" and "clouds" fields were taken into account. HO_2 data were seen as the day-minus-night difference as prescribed by the MLS data guidelines (Livesey et al., 2017). Following Pickett et al. (2008), each daytime profile of this component measured on a given day at a latitude Lat, a profile resulting from averaging the nighttime profiles of HO_2, measured on the same day in the latitude range of Lat±5°, was subtracted. This operation

eliminates systematic biases affecting HO_2 retrievals, but limits the studied latitude range to the one where MLS observes both daytime and nighttime data.

The integrals in Eq. (~~20~~ 12)–(~~21~~ 13) were calculated at every pressure level p for each set of simultaneously measured vertical profiles $OH^{MLS}(p)$, $HO_2^{MLS}(p)$, $O_3^{MLS}(p)$, $T^{MLS}(p)$, $\sigma_{OH^{MLS}}(p)$, $\sigma_{HO_2^{MLS}}(p)$, $\sigma_{O_3^{MLS}}(p)$. The vertical profiles ~~$<OH^r>(p)$~~ $<OH^{ret}>(p)$, ~~$<HO_2^r>(p)$~~ $<HO_2^{ret}>(p)$, ~~$<O_3^r>(p)$~~ $<O_3^{ret}>(p)$, ~~$\sigma_{OH^r}(p)$~~ $\sigma_{OH^{ret}}(p)$, ~~$\sigma_{HO_2^r}(p)$~~ $\sigma_{HO_2^{ret}}(p)$, ~~$\sigma_{O_3^r}(p)$~~ $\sigma_{O_3^{ret}}(p)$ were found at each point of the globe along the satellite track. Numerical integration was performed by a Monte Carlo method. For each pressure level, a sample of about $5\cdot10^5$ pairs of random variable values ~~$\{u_1, u_2\} = \{HO_2^r, O_3^r\}$~~ $\{u_1, u_2\} = \{HO_2^{ret}, O_3^{ret}\}$ distributed with normalized probability density given by Eq. (~~19~~11) with $P_{apr}(u_1,u_2) \equiv 1$ was generated with the help of the Metropolis-Hastings algorithm (Chib and Greenberg, 1995). In this case, the statistical moments in Eq. (~~20) (21~~12)–(13) were determined by summation over the sample.

A typical example of retrieved profiles ~~HO_2^r, O_3^r and OH^r~~ HO_2^{ret}, O_3^{ret} and OH^{ret} (black curves) in comparison with the measured HO_2^{MLS}, O_3^{MLS} and OH^{MLS} (red curves) is given in Fig. ~~2~~4. First of all, note that statistics of the retrieved data is in satisfactory agreement with the initial measurement of OH and O_3 concentrations, but not of HO_2. The error of satellite measurement, $\sigma_{HO_2^{MLS}}$, greatly exceeds the uncertainty of retrieval, ~~$\sigma_{HO_2^r}$~~ $\sigma_{HO_2^{ret}}$, so at some altitudes the values of $<HO_2^{MLS}>$ (red dashed curves) do not fall within the corresponding intervals ~~$<HO_2^r> \pm \sigma_{HO_2^r}$~~ $<HO_2^{ret}> \pm \sigma_{HO_2^{ret}}$. Second, the results of a single measurement of all three components and their retrieved values have considerable uncertainties relative to their means within the whole interval of altitudes. Therefore, the observed and retrieved data should be compared using the commonly accepted approach (e.g., Pickett et al., 2008) of averaging large ensembles of profiles within certain latitude and time ranges, or zones. It is supposed that the noise of satellite measurement instruments is delta-correlated, so that random values corresponding to each single measured or retrieved profile are statistically independent. In this case the dispersion of a measured or retrieved zonal mean profile is determined by summation

$$\sigma^2_{\Sigma} = \frac{1}{N^2}\sum_{k=1}^{N}\sigma^2_k ,$$

where N is the number of measured or retrieved profiles within the zone and σ^2_k is the dispersion of the k-th measured or retrieved profile.

The range of latitudes ~~±82° N~~ covered by the satellite trajectory was divided into ~~16 equal zones~~ 17 bins 10^0 each. About 3000 single profiles of each chemical component fall into one ~~zone~~ bin during ~~each~~ a month of MLS/Aura observations. Therefore, the resulting uncertainties due to measurement noise of OH, HO_2 and O_3 concentration profiles (both measured and retrieved) averaged over such ensembles are significantly (about one and a half order of magnitude) lower than the uncertainties of individual profiles. Examples of such profiles for January, May and September 2005 are presented in Fig. ~~3~~ 5. One can see that the indicated uncertainties are now small enough to make clear conclusions about the extent to which the observed and retrieved profiles agree by comparing their averaged values only, i.e. $<OH^{MLS}>$, $<HO_2^{MLS}>$, $<O_3^{MLS}>$ and ~~$<OH^{r}>$~~ $<OH^{ret}>$, ~~$<HO_2^{r}>$~~ $<HO_2^{ret}>$, ~~$<O_3^{r}>$~~ $<O_3^{ret}>$.

Figures ~~4~~6–~~6~~8 show monthly averaged zonal mean pressure–latitude cross-sections of ~~$<HO_2^{r}>$~~ $<HO_2^{ret}>$, $<HO_2^{MLS}>$, ~~$\Delta HO_2 = (<HO_2^{r}> - <HO_2^{MLS}>)/<HO_2^{MLS}>$~~ $\Delta HO_2 = (<HO_2^{ret}> - <HO_2^{MLS}>)/<HO_2^{MLS}>$ and similar characteristics for OH and O_3 concentration profiles for three months of the year 2005. ~~First, clearly, the distributions of $<OH^{r}>$ and $<O_3^{r}>$ are in good qualitative and quantitative agreement with the initial MLS/Aura measurement data at lower altitudes, below ~ 0.1 hPa. At higher altitudes, the distributions of $<OH^{r}>$ reproduce all the main structural features of $<OH^{MLS}>$ except for a small 2–3 km downward displacement of the OH layer. Moreover, at these altitudes the retrieved OH concentration has lower values than the observed one with a relative difference ΔOH reaching several tens of percent at altitudes above ~ 0.05 hPa. The distribution of $<O_3^{r}>$ above 0.1 hPa, in turn, differs considerably from $<O_3^{MLS}>$, both in quantity and quality, especially within the 0.003–0.05 hPa altitude interval, where ΔO_3 locally reaches several times. Second, for all months there are significant qualitative and quantitative differences between $<HO_2^{r}>$ and $<HO_2^{MLS}>$, the most noticeable one being location of the mesospheric maximum of this component's concentration.~~

~~According to the observations it is close to 0.1 hPa, while the retrieved data demonstrates the altitude of about 0.05 hPa.~~ First, clearly, the distributions of $<OH^{ret}>$ and $<O_3^{ret}>$ are in good qualitative and quantitative agreement with the initial MLS/Aura measurement data at lower altitudes, below ~ 0.07 mbar and 0.1 mbar, correspondingly. At higher altitudes, the distributions of $<OH^{ret}>$ reproduce all the main structural features of $<OH^{MLS}>$, but the retrieved OH concentration has lower values than the observed one with a relative difference ΔOH reaching ~15% at the top. The distribution of $<O_3^{ret}>$ above 0.1 mbar, in turn, differs considerably from $<O_3^{MLS}>$, both in quantity and quality, and ΔO_3 locally reaches 50-60% and more. Second, for all months there are significant qualitative and quantitative differences between $<HO_2^{ret}>$ and $<HO_2^{MLS}>$, the most noticeable one being location of the mesospheric maximum of this component's concentration. According to the observations it is close to 0.1 mbar, while the retrieved data demonstrate the altitudes of about ~0.046 mbar or higher. Our analysis of the applied method of statistical evaluation demonstrates that the higher position of this maximum in the distributions of $<HO_2^{ret}>$ is influenced by the OH^{MLS} data in which the mesospheric maximum (see Figs. 6-8) is also located notably higher than 0.1 mbar.

6. Discussion and conclusion

On the basis of the data presented in Section 5 we can conclude that, upon the whole, simultaneous OH, HO_2 and O_3 satellite measurements poorly satisfy the photochemical equilibrium condition. The HO_2 component biases from this condition most prominently. We can conjecture that a possible explanation for the bias is the significant systematic error in HO_2 measurements, in particular, in the height of the mesospheric maximum. ~~The discrepancy between the measured and real HO_2, in turn, impacts the retrieved data for OH and O_3 and, above 0.1 hPa, leads to a significant mismatch between the averaged retrieved values ($<OH^r>$, $<O_3^r>$) and averaged measured values ($<OH^{MLS}>$, $<O_3^{MLS}>$).~~ This assumption is supported by the calculation of the HO_2 distributions with the use of our 3D chemical transport model (see Fig. 9). It can be seen that the mesospheric maximum of HO_2 in these months, as well as of the $<HO_2^{ret}>$ distributions, lies

above 0.046 mbar.

~~EOS MLS data quality and description document (Livesey et al., 2017) states that scientifically useful pressure range for HO_2 measurements is 22 – 0.046 hPa. Exclusion from Figs. 4-6 of the range above 0.046 hPa diminishes the mismatch for OH and O_3 but not for HO_2. An algorithm for offline retrieval of daily zonal means of HO_2 using averaged MLS radiances was performed by Millán et al. (2015). The product of the algorithm, the alternative dataset of night-time and daytime HO_2, recently became available at https://mls.jpl.nasa.gov. Figure 7 shows the monthly averaged zonal means from the dataset ($<HO_2^{MLS}_{offline}>$) corresponding to Figs. 4-6. Figure 7 depicts the same monthly means as Figures 4-6. One can see that the results of the offline HO_2 retrieval show the same features as the results of our evaluation technique as compared to standard MLS retrieval: the height of mesospheric HO_2 maximum is higher. It is worth noting that the positions of the maximum in $<HO_2^{r}>$ and $<HO_2^{MLS}_{offline}>$ distributions are close. For detailed qualitative and quantitative comparison of $<HO_2^{r}>$ and $<HO_2^{MLS}_{offline}>$ one should use the evaluation procedure technique for zonally averaged all three MLS components, which requires significant modification of the procedure and is beyond the scope of this technical Note.~~

Moreover, new data on the HO_2 distributions were recently obtained from the MLS measurements. Millán et al. (2015) performed the offline retrieval of daily zonal means of HO_2 profiles using averaged MLS radiances measured in 10° latitude bins. Averaged spectra have a better signal to noise ratio, which removes many of the limitations of the MLS standard product for HO_2. In particular, the upper boundary of the altitude region in which daytime data is suitable for scientific use has reached 0.0032 mbar, and the "day-minus-night" correction is not needed at altitudes above 1 mbar. Comparison with various experimental and model data has shown that the offline retrieval reproduces the basic properties of the HO_2 distribution in the mesosphere relatively well (at least qualitatively) (Millán et al. 2015).

The offline retrieval product, the alternative dataset of daytime HO_2, has recently become publicly available at https://mls.jpl.nasa.gov. Figure 10 shows the monthly averaged zonal means of offline retrieval data ($<HO_2^{MLS}_{offline}>$) and relative differences with retrieved and MLS standard product data $(<HO_2^{MLS}> - <HO_2^{MLS}_{offline}>)/ <HO_2^{MLS}_{offline}>$ and $(<HO_2^{ret}> - <HO_2^{MLS}_{offline}>)/ <HO_2^{MLS}_{offline}>$, correspondingly. Figure 10 represents the same time

periods as Figs. 6-8. It is worth noting that the distributions $<HO_2^{MLS}{}_{offline}>$ depicted in Fig. 10 represent significantly different amounts of data. The data sets for May and September include 31 and 27 days of measurements, respectively, whereas the January dataset encompasses only 4 days. The latter makes the graphs in the first row in Fig. 10 noisier than the others. One can see that the results of the offline HO_2 retrieval show the same features as the results of our evaluation technique in comparison to the standard MLS retrieval, i.e. the height of mesospheric HO_2 maximum is notably higher. We can conclude that the distributions of $<HO_2^{ret}>$ better match $<HO_2^{MLS}{}_{offline}>$ than $<HO_2^{MLS}>$, although some quantitative discrepancy between $<HO_2^{ret}>$ and $<HO_2^{MLS}{}_{offline}>$ also exists. Note that this may be due to systematic errors in the HO_2^{MLS} distributions, which cannot be excluded within the framework of the introduced technique. For a detailed qualitative and quantitative comparison of $<HO_2^{ret}>$ and $<HO_2^{MLS}{}_{offline}>$ one should modify the method, so that a statistical evaluation of the OH^{MLS} and O_3^{MLS} standard products, and the data of the offline HO_2 retrieval could be conducted within the framework of a single procedure with no account for the HO_2^{MLS} distributions. This modification is under way and will be presented elsewhere.

The proposed method for statistical evaluation of mesospheric species measurements can be readily generalized to other atmospheric photochemical systems that contain short ~~-lifetime-~~lived components (see ~~the~~ Introduction). It may also be modified for assessing hard to measure chemical components, characteristics of atmospheric processes (like wind speed or turbulent diffusion rate), or poorly known reaction rates. ~~Such evaluation will be correct from the statistical point of view.~~

Acknowledgments

This work was supported by the Russian Science Foundation (contract No. 15–17–10024 of June 04, 2015). The data used in this study is supported by the Institute of Applied Physics of the Russian Academy of Sciences (Nizhny Novgorod, Russia). Inquiries about ~~calculated~~ the distributions used ~~for~~ in this paper can be addressed to Mr. Belikovich (belikovich@ipfran.ru).

References

Avallone, L. M., and Toohey, D. W.: Tests of halogen photochemistry using in situ measurements of ClO and BrO in the lower polar stratosphere, J. Geophys. Res., Volume 106, Issue D10, Pages 10411–1042, doi: 10.1029/2000JD900831, 2001.

Benton, A. K., Langridge, J. M., Ball, S. M., Bloss, W. J., Dall'Osto, M., Nemitz, E., Harrison, R. M., and Jones, R. L.: Night-time chemistry above London: measurements of NO3 and N2O5 from the BT Tower, Atmos. Chem. Phys., 10, 9781-9795, doi:10.5194/acp-10-9781-2010, 2010.

Berger, U.: Numerische Simulation klimatologischer Prozesse und thermische Gezeiten in der mittleren Atmosph¨are, Thesis, Univ. Cologne, Germany, 1994.

Berger, U. and von Zahn, U.: The two-level structure of the mesopause: A model study, J. Geophys. Res., 104, 22083–22093, 1999.

Berthet, G., Ricaud, P., Lefevre, F., Le Flochmoen, E., Urban, J., Barret, B., Lautie, N., Dupuy, E., De La Noe, J., and Murtagh, D.: Nighttime chlorine monoxide observations by the Odin satellite and implications for the ClO/Cl_2O_2 equilibrium, Geophys. Res. Lett., 32, L11812, doi:10.1029/2005GL022649, 2005.

Brasseur, G. and Solomon, S.: Aeronomy of the Middle Atmosphere, 644 pp., 3rd edition, Springer, The Netherlands, 2005.

Brown, S. S., Stark, H., Ryerson, T. B., Williams, E. J., Nicks Jr., D. K., Trainer, M., Fehsenfeld, F. C., and Ravishankara, A. R.: Nitrogen oxides in the nocturnal boundary layer: Simultaneous in situ measurements of NO_3, N_2O_5, NO_2, NO, and O_3, J. Geophys. Res., 108(D9), 4299, doi:10.1029/2002JD002917, 2003.

Burkholder, J. B., S. P. Sander, J. Abbatt, J. R. Barker, R. E. Huie, C. E. Kolb, M. J. Kurylo, V. L. Orkin, D. M. Wilmouth, and P. H. Wine (2015), Chemical Kinetics and Photochemical Data for Use in Atmospheric Studies, Evaluation No. 18, JPL Publication 15-10, Jet Propulsion Laboratory, Pasadena, http://jpldataeval.jpl.nasa.gov.

Butz, A., H. Bosch, C. Camy-Peyret, M. Dorf, A. Engel, S. Payan, and Pfeilsticker, K.: Observational constraints on the kinetics of the ClO-BrO and ClO-ClO ozone loss cycles in the Arcticwinter stratosphere, Geophys. Res. Lett., 34, L05801, doi:10.1029/2006GL028718, 2007.

Cantrell, C. A., Mauldin, L., Zondlo, M., Eisele, F., Kosciuch, E., Shetter, R., Lefer, B., Hall, S., Campos, T., Ridley, B., Walega, J., Fried, A., Wert, B., Flocke, F., Weinheimer, A., Hannigan,

J., Coffey, M., Atlas, E., Stephens, S., Heikes, B., Snow, J., Blake, D., Blake, N., Katzenstein, A., Lopez, J., Browell, E. V., Dibb, J., Scheuer, E., Seid, G., and Talbot, R.: Steady state free radical budgets and ozone photochemistry during TOPSE, J. Geophys. Res., 108(D4), 8361, doi:10.1029/2002JD002198, 2003.

Chameides, W.: Tropospheric odd nitrogen and the atmospheric water vapor cycle, J. Geophys. Res., 84 (C10), 4989–4996, doi: 10.1029/JC080i036p04989, 1975.

Chib, S., and Greenberg, E.: Understanding the Metropolis-Hastings Algorithm, The American Statistician, 49 (4), 327-335, doi: 10.2307/2684568, 1995.

Crawford, J., Davis, D., Chen, G., Bradshaw, J., Sandholm, S., Gregory, G., Sachse, G., Anderson, B., Collins, J., Blake, D., Singh, H., Heikes, B., Talbot, R., Rodriguez, J.: Photostationary state analysis of the NO_2-NO system based on airborne observations from the western and central North Pacific, 101(D1), 2053–2072, doi: 10.1029/95JD02201, 1996.

Crowley, J. N., Schuster, G., Pouvesle, N., Parchatka, U., Fischer, H., Bonn, B., Bingemer, H., and Lelieveld, J.: Nocturnal nitrogen oxides at a rural mountain-site in south-western Germany, Atmos. Chem. Phys., 10, 2795-2812, doi:10.5194/acp-10-2795-2010, 2010.

de Grandpre, J., Beagley, S. R., Fomichev, V. I., Griffioen, E., McConnell, J. C., Medvedev, A. S., and Shepherd., T. G.: Ozone climatology using interactive chemistry: Results from the Canadian Middle Atmosphere Model, J. Geophys. Res.-Atmos., 105, 26475-26491, doi:10.1029/2000JD900427, 2000.

Djouad, R., Michelangeli, D. V., and Gong, W.: Numerical solution for atmospheric multiphase models: Testing the validity of equilibrium assumptions, J. Geophys. Res., 108(D19), 4602, doi:10.1029/2002JD002969, 2003.

Douglass, A. R., Jackman, C. H., and Stolarski, R. S.: Comparison of model results transporting the odd nitrogen family with results transporting separate odd nitrogen species, J. Geophys. Res., 94(D7), 9862–9872, doi:10.1029/JD094iD07p09862, 1989.

Ebel, A., Berger, U., and Krueger, B. C.: Numerical simulations with COMMA, a global model of the middle atmosphere, SIMPO Newsletter, 12, 22–32, 1995.

Evans, W. F. J., and Llewellyn, E. J.: Atomic hydrogen concentrations in the mesosphere and the hydroxyl emissions, J. Geophys. Res., 78, 323–326, doi:10.1029/JA078i001p00323, 1973.

Evans, W.F.J., McDade, I. C., Yuen, J., and Llewellyn, E. J.: A rocket measurement of the O_2 infrared atmospheric (0-0) band emission in the dayglow and a determination of the

mesospheric ozone and atomic oxygen densities, Can. J. Phys., 66, 941–946, doi:10.1139/p88-15, 1988.

Feigin, A. M., and Konovalov, I. B.: On the possibility of complicated dynamic behavior of atmospheric photochemical systems: Instability of the Antarctic photochemistry during the ozone hole formation, J. Geophys. Res., 101, 26023–26038, doi:10.1029/96JD02011, 1996.

Feigin, A. M., Konovalov, I. B., and Molkov, Ya. I.: Towards understanding nonlinear nature of atmospheric photochemistry: Essential dynamic model of the mesospheric photochemical system, J. Geophys. Res., 103, 25447–25460, doi:10.1029/98JD01569, 1998.

Funke, B., Lopez-Puertas, M., von Clarmann, T., Stiller, G. P., Fischer, H., Glatthor, N., Grabowski, U., Hopfner, M., Kellmann, S., Kiefer, M., Linden, A., Mengistu Tsidu, G., Milz, M., Steck, T. and Wang, D. Y.: Retrieval of stratospheric NOx from 5.3 and 6.2 mm nonlocal thermodynamic equilibrium emissions measured by Michelson Interferometer for Passive Atmospheric Sounding (MIPAS) on Envisat, J. Geophys. Res., 110, D09302, doi:10.1029/2004JD005225, 2005.

Ghosh, S., Pyle, J. A., and Good, P.: Temperature dependence of the ClO concentration near the stratopause, J. Geophys. Res., 102(D15), 19207–19216, doi:10.1029/97JD01099, 1997.

Good, R. E.: Determination of atomic oxygen density from rocket borne measurements of hydroxyl airglow, Planet. Space Sci., 24, 389–395, doi.org/10.1016/0032-0633(76)90052-0, 1976.

~~Grygalashvyly, M.: Several notes on the OH* layer, Ann. Geophys., 33, 923-930, doi:10.5194/angeo-33-923-2015, 2015.~~

Grygalashvyly, M., Sonnemann, G. R., and Hartogh, P.: Long-term behavior of the concentration of the minor constituents in the mesosphere—A model study, Atmos. Chem. Phys., 9, 2779–2792, doi:10.5194/acp-9-2779-2009, 2009.

Grygalashvyly, M., Becker, E., and Sonnemann, G. R.: Wave mixing effects on minor chemical constituents in the MLT region: Results from a global CTM driven by high-resolution dynamics, J. Geophys. Res., 116, D18302, doi:10.1029/2010JD015518, 2011.

Grygalashvyly, M., Becker, E., and Sonnemann, G. R.: Gravity wave mixing and effective diffusivity for minor chemical constituents in the mesosphere/lower thermosphere, Space Sci. Rev., 168, 333–362, doi:10.1007/s11214-011-9857-x, 2012.

Grygalashvyly, M., Sonnemann, G. R., Lübken, F.-J., Hartogh, P., and Berger, U.: Hydroxyl layer: Mean state and trends at midlatitudes, J. Geophys. Res.-Atmos., 119, 12391–12419, doi:10.1002/2014JD022094, 2014.

Grygalashvyly, M.: Several notes on the OH* layer, Ann. Geophys., 33, 923-930, doi:10.5194/angeo-33-923-2015, 2015.

Hartogh, P., Jarchow, C., Sonnemann, G. R., and Grygalashvyly, M.: On the spatiotemporal behavior of ozone within the upper mesosphere/mesopause region under nearly polar night conditions, J. Geophys. Res., 109, D18303, doi:10.1029/2004JD004576, 2004.

Hartogh, P., Sonnemann, G. R., Grygalashvyly, M., and Jarchow, Ch.: Ozone trends in mid-latitude stratopause region based on microwave measurements at Lindau (51.66° N, 10.13° E), the ozone reference model, and model calculations, Adv. Space Res., 47, 1937-1948, doi:10.1016/j.asr.2011.01.010, 2011.

Hauchecorne, A., Bertaux, J. L., Dalaudier, F., Keckhut, P., Lemennais, P., Bekki, S., Marchand, M., Lebrun, J. C., Kyrölä, E., Tamminen, J., Sofieva, V., Fussen, D., Vanhellemont, F., Fanton d'Andon, O., Barrot, G., Blanot, L., Fehr, T., and Saavedra de Miguel, L.: Response of tropical stratospheric O_3, NO_2 and NO_3 to the equatorial Quasi-Biennial Oscillation and to temperature as seen from GOMOS/ENVISAT, Atmos. Chem. Phys., 10, 8873-8879, doi:10.5194/acp-10-8873-2010, 2010.

Jackman, C. H., Marsh, D. R., Vitt, F. M., Roble, R. G., Randall, C. E., Bernath, P. F., Funke, B., López-Puertas, M., Versick, S., Stiller, G. P., Tylka, A. J., and Fleming, E. L.: Northern Hemisphere atmospheric influence of the solar proton events and ground level enhancement in January 2005, Atmos. Chem. Phys., 11, 6153-6166, https://doi.org/10.5194/acp-11-6153-2011, 2011.

Jackman, C. H., Randall, C. E., Harvey, V. L., Wang, S., Fleming, E. L., López-Puertas, M., Funke, B., and Bernath, P. F.: Middle atmospheric changes caused by the January and March 2012 solar proton events, Atmos. Chem. Phys., 14, 1025-1038, https://doi.org/10.5194/acp-14-1025-2014, 2014.

Kawa, S. R., Fahey, D. W., Solomon, S., Brune, W. H., Proffitt, M. H., Toohey, D. W., Anderson Jr., D. E., Anderson, L. C., and Chan, K. R.: Interpretation of aircraft measurements of NO, ClO, and O_3 in the lower stratosphere, J. Geophys. Res., 95(D11), 18597–18609 doi: 10.1029/JD095iD11p18597, 1990.

Kremp, C., Berger, U., Hoffmann, P., Keuer, D., and Sonnemann, G. R.: Seasonal variation of middle latitude wind fields of the mesopause region – a comparison between observation and model calculation, Geophys. Res. Lett., 26, 1279–1282, 1999.

Kaye, J. A., and Rood, R. B.: Chemistry and transport in a three-dimensional stratospheric model: Chlorine species during a simulated stratospheric warming, J. Geophys. Res., 94(D1), 1057–1083, doi: 10.1029/JD094iD01p01057, 1989.

Ko, M., Hu, W., Rodriguez, J. M., Kondo, Y., Koike, M., Kita, K., Kawakami, S., Blake, D., Liu, S., and Ogawa, T.: Photochemical ozone budget during the BIBLE A and B campaigns, J. Geophys. Res., 107, 8404, doi:10.1029/2001JD000800, 2002. [printed 108(D3), 2003].

Kondo, Y., Matthews, W. A., Aimedieu, P., and Robbins, D. E. Diurnal variation of nitric oxide at 32 km: Measurements and interpretation, J. Geophys. Res., 93(D3), 2451–2460, doi:10.1029/JD093iD03p02451, 1988.

Kondo, Y., Ziereis, H., Koike, M., Kawakami, S., Gregory, G. L., Sachse, G. W., Singh, H. B., Davis, D. D., Merrill, J. T.: Reactive nitrogen over the Pacific Ocean during PEM-West, A 101(D1), 1809–1828, doi:10.1029/95JD02611, 1996.

Konovalov, I. B., Feigin, A. M., Mukhina, A. Y.: Toward understanding of the nonlinear nature of atmospheric photochemistry: Multiple equilibrium states in the high-latitude lower stratospheric photochemical system, J. Geophys. Res, 104, 8669-8689, doi:10.1029/1998JD100037, 1999.

Konovalov, I. B., and Feigin, A. M.: Toward an understanding of the nonlinear nature of atmospheric photochemistry: Origin of the complicated dynamic behaviour of the mesospheric photochemical system, Nonlin. Processes Geophys., 7, 87–104, doi:10.5194/npg-7-87-2000, 2000.

Körner, U., and Sonnemann, G. R.: Global 3D-modeling of water vapor concentration of the mesosphere/mesopause region and implications with respect to the NLC region, J. Geophys. Res.-Atmos., 106, 9639– 9651, doi:10.1029/2000JD900744, 2001.

Kowalewski, S., von Savigny, C., Palm, M., McDade, I. C., and Notholt, J.: On the impact of the temporal variability of the collisional quenching process on the mesospheric OH emission layer: a study based on SD-WACCM4 and SABER, Atmos. Chem. Phys., 14, 10193-10210, doi:10.5194/acp-14-10193-2014, 2014.

Kremser, S., Schofield, R., Bodeker, G. E., Connor, B. J., Rex, M., Barret, J., Mooney, T., Salawitch, R. J., Canty, T., Frieler, K., Chipperfield, M. P., Langematz, U., and Feng, W.: Retrievals

of chlorine chemistry kinetic parameters from Antarctic ClO microwave radiometer measurements, Atmos. Chem. Phys., 11, 5183-5193, doi:10.5194/acp-11-5183-2011, 2011.

Kulikov, M. Y., Feigin, A. M., and Sonnemann, G. R.: Retrieval of the vertical distribution of chemical components in the mesosphere from simultaneous measurements of ozone and hydroxyl distributions, Radiophys. Quantum Electron., 49, 683–691, doi:10.1007/s11141-006-0103-4, 2006.

Kulikov, M. Yu., Feigin, A. M., and Sonnemann, G. R.: Retrieval of water vapor profile in the mesosphere from satellite ozone and hydroxyl measurements by the basic dynamic model of mesospheric photochemical system, Atmos. Chem. Phys., 9, 8199-8210, doi:10.5194/acp-9-8199-2009, 2009.

Kulikov, M. Y., Mukhin, D. N., and Feigin, A. M.: Bayesian strategy of accuracy estimation for characteristics retrieved from experimental data using base dynamic models of atmospheric photochemical systems, Radiophys. Quantum Electron., 52, 618–626, doi:10.1007/s11141-010-9171-6, 2009.

Kulikov, M. Yu., Vadimova, O. L., Ignatov, S. K., and Feigin, A.M.: The mechanism of non-linear photochemical oscillations in the mesopause region, Nonlinear Processes in Geophysics, v.19, p.p.501–512, doi:10.5194/npg-19-501-2012, 2012.

Kulikov, M. Yu., and Feigin, A. M.: Automated construction of the basic dynamic models of the atmospheric photochemical systems using the RADM2 chemical mechanism as an example, Radiophys. Quantum Electron., 57, 478-487, doi 10.1007/s11141-014-9530-9, 2014.

Kulikov, M. Y., Belikovich, M. V., Grygalashvyly, M., Sonnemann, G. R., Ermakova, T. S., Nechaev, A. A., and Feigin, A. M.: Daytime ozone loss term in the mesopause region, Ann. Geophys., 35, 677-682, doi:10.5194/angeo-35-677-2017, 2017.

~~Livesey, N. J., et al., EOS MLS version 4.2x Level 2 data quality and description document, Tech. rep., Jet Propulsion Laboratory, D-33509 Rev. C, available from https://mls.jpl.nasa.gov/data/v4-2_data_quality_document.pdf, 2017.~~

Livesey, N. J., Read, W. G., Wagner, P. A., Frovideaux, L., Lambert, A., Manney, G. L., Millan, L. F., Pumphrey, H. C., Santee, M. L., Schwartz, M. J., Wang, S., Fuller, R. A., Jarnot, R. F., Knosp, B. W., and Martinez E.: Earth Observing System (EOS) Aura Microwave Limb Sounder (MLS) Version 4.2 Level 2 data quality and description document, JPL D-33509, JPL publication, USA, 2017.

692 Llewellyn, E. J., McDade, I. C., Moorhouse, P., and Lockerbie, M. D.: Possible reference
693 models for atomic oxygen in the terrestrial atmosphere, Adv. Space Res., 13, 135–144,
694 doi:0.1016/0273-1177(93)90013-2, 1993.
695 Llewellyn, E. J., and McDade, I. C.: A reference model for atomic oxygen in the terrestrial
696 atmosphere, Adv. Space Res., 18, 209–226, doi:10.1016/0273-1177(96)00059-2, 1996.
697 Lubken, F. J.: Seasonal variation of turbulent energy dissipation rates at high latitudes as
698 determined by in situ measurements of neutral density fluctuations, J. Geophys. Res., 102, 13441–
699 13456, 1997.
700 Marchand, M., Bekki, S., Lefevre, F., and Hauchecorne, A.: Temperature retrieval from
701 stratospheric O3 and NO3 GOMOS data, Geophys. Res. Lett., 34, L24809,
702 doi:10.1029/2007GL030280, 2007.
703 Marsh, D. R., Smith, A. K., Mlynczak, M. G., and Russell III, J. M.: SABER observations of
704 the OH Meinel airglow variability near the mesopause, J. Geophys. Res., 111, A10S05,
705 doi:10.1029/2005JA011451, 2006.
706 Martinez, M., Perner, D., Hackenthal, E.-M., Kulzer, S., and Schultz, L.: NO_3 at Helgoland
707 during the NORDEX campaign in October 1996, J. Geophys. Res., 105(D18), 22,685–22,695,
708 doi:10.1029/2000JD900255, 2000.
709 Massie, S. T., and Hunten, D. M.: Stratospheric eddy diffusion coefficients from tracer data,
710 J. Geophys. Res., 86(C10), 9859–9868, doi:10.1029/JC086iC10p09859, 1981.
711 McDade, I. C., Llewellyn, E. J., and Harris, F. R.: Atomic oxygen concentrations in the lower
712 auroral thermosphere, Adv. Space Res., 5(7), 229–232, doi:10.1016/0273-1177(85)90379-5, 1985.
713 McDade, I. C., and Llewellyn, E. J.: Mesospheric oxygen atom densities inferred from night-
714 time OH Meinel band emission rates, Planet. Space Sci., 36, 897–905, DOI:10.1016/0032-
715 0633(88)90097-9, 1988.
716 McLaren, R., Wojtal, P., Majonis, D., McCourt, J., Halla, J. D., and Brook, J.: NO_3 radical
717 measurements in a polluted marine environment: links to ozone formation, Atmos. Chem. Phys.,
718 10, 4187-4206, doi:10.5194/acp-10-4187-2010, 2010.
719 Millán, L., Wang, S., Livesey, N., Kinnison, D., Sagawa, H., and Kasai, Y.: Stratospheric and
720 mesospheric HO_2 observations from the Aura Microwave Limb Sounder, Atmos. Chem. Phys., 15,
721 2889-2902, doi:10.5194/acp-15-2889-2015, 2015.

Mlynczak, M. G., and Solomon, S.: Middle atmosphere heating by exothermic chemical reactions involving odd-hydrogen species, Geophys. Res. Lett., 18, 37-40, doi:10.1029/90GL02672, 1991.

Mlynczak, M. G., and Solomon, S.: A detailed evaluation of the heating efficiency in the middle atmosphere, J. Geophys. Res., 98, 10,517–10,541, doi:10.1029/93JD00315, 1993.

Mlynczak, M. G., Marshall, B. T., Martin-Torres, F. J., Russell III, J. M., Thompson, R. E., Remsberg, E. E., and Gordley, L. L.: Sounding of the Atmosphere using Broadband Emission Radiometry observations of daytime mesospheric O2(1D) 1.27 μm emission and derivation of ozone, atomic oxygen, and solar and chemical energy deposition rates, J. Geophys. Res., 112, D15306, doi:10.1029/2006JD008355, 2007.

Mlynczak, M. G., Hunt, L. A., Mast, J. C., Marshall, B. T., Russell III, J. M., Smith, A. K., Siskind, D. E., Yee, J.-H., Mertens, C. J., Martin-Torres, F. J., Thompson, R. E., Drob, D. P., and Gordley, L. L.: Atomic oxygen in the mesosphere and lower thermosphere derived from SABER: Algorithm theoretical basis and measurement uncertainty, J. Geophys. Res., 118, 5724–5735, doi:10.1002/jgrd.50401, 2013a.

Mlynczak, M. G., Hunt, L. H., Mertens, C. J., Marshall, B. T., Russell III, J. M., López-Puertas, M., Smith, A. K., Siskind, D. E., Mast, J. C., Thompson, R. E., and Gordley, L. L.: Radiative and energetic constraints on the global annual mean atomic oxygen concentration in the mesopause region, J. Geophys. Res. Atmos., 118, 5796–5802, doi:10.1002/jgrd.50400, 2013b.

Mlynczak, M. G., Hunt, L. A., Marshall, B. T., Mertens, C. J., Marsh, D. R., Smith, A. K., Russell, J. M., Siskind, D. E., and Gordley, L. L.: Atomic hydrogen in the mesopause region derived from SABER: Algorithm theoretical basis, measurement uncertainty, and results, J. Geophys. Res., 119, 3516–3526, doi:10.1002/2013JD021263, 2014.

Morton, K. W., and D. F. Mayers, Numerical Solution of Partial Differential Equations, Cambridge University Press, 1994.

Nechaev, A. A., Ermakova, T. S., and Kulikov, M. Y.: Determination of the Trace-Gas Concentrations at the Altitudes of the Lower and Middle Mesosphere from the Time Series of Ozone Concentration, Radiophys. Quantum Electron., 59, 546–559, doi:10.1007/s11141-016-9722-6, 2016.

751 Nikoukar, R., Swenson, G. R., Liu, A. Z., and Kamalabadi, F.: On the variability of
752 mesospheric OH emission profiles, J. Geophys. Res., 112, D19109, doi:10.1029/2007JD008601,
753 2007.
754 Pendleton, W. R., Baker, K. D., and Howlett, L. C.: Rocket-based investigations of $O(^3P)$,
755 $O_2(a^1\Delta_g)$ and OH*($\nu=1,2$) during the solar eclipse of 26 February1979, J. Atm. Terr. Phys., 45 (7),
756 479 – 491, doi:10.1016/S0021-9169(83)81108-8, 1983.
757 Penkett, S. A., Monks, P. S., Carpenter, L. J., Clemitshaw, K. C., Ayers, G. P., Gillett, R. W.,
758 Galbally, I. E., and Meyer, C. P.: Relationships between ozone photolysis rates and peroxy radical
759 concentrations in clean marine air over the Southern Ocean, J. Geophys. Res., 102(D11), 12805–
760 12817, doi:10.1029/97JD00765, 1997.
761 Penkett, S. A., Reeves, C. E., Bandy, B. J., Kent, J. M., and Richer, H. R.: Comparison of
762 calculated and measured peroxide data collected in marine air to investigate prominent features of
763 the annual cycle of ozone in the troposphere, J. Geophys. Res., 103(D11), 13377–13388,
764 doi:10.1029/97JD02852, 1998.
765 Platt, U., Perner, D., and Pätz, H. W.: Simultaneous measurement of atmospheric CH2O,
766 O3, and NO2 by differential optical absorption, J. Geophys. Res., 84(C10), 6329–6335,
767 10.1029/JC084iC10p06329, 1979.
768 Pyle, J. A., Zavody, A. M., Harries, J. E., and Moffat, P. H.: Derivation of OH concentration
769 from satellite infrared measurements of NO_2 and HNO_3, Nature, 305, 690-692,
770 doi:10.1038/305690a0, 1983.
771 Pyle, J. A., and Zavody, A. M.: The derivation of hydrogen containing radical concentrations
772 from satellite data sets, Q. J. R. Meteorol. Soc., 111, 993-1012, doi:10.1002/qj.49711147005,
773 1985.
774 Pickett, H. M., and Peterson, D. B.: Comparison of measured stratospheric OH with
775 prediction, J. Geophys. Res., 101(D11), 16789–16796, doi: 10.1029/96JD01168, 1996.
776 Pickett, H. M., Drouin, B. J., Canty, T., Salawitch, R. J., Fuller, R. A., Perun, V. S., Livesey,
777 N. J., Waters, J. W., Stachnik, R. A., Sander, S. P., Traub, W. A., Jucks, K. W., and Minschwaner,
778 K.: Validation of Aura Microwave Limb Sounder OH and HO2 measurements, J. Geophys. Res.,
779 113, D16S30, doi:10.1029/2007JD008775, 2008.

Rasch, P. J., Boville, B. A., and Brasseur, G. P.: A three-dimensional general circulation model with coupled chemistry for the middle atmosphere, J. Geophys. Res., 100(D5), 9041–9071, doi: 10.1029/95JD00019, 1995.

Russell, J. P., and Lowe, R. P.: Atomic oxygen profiles (80–94 km) derived from Wind Imaging Interferometer/Upper Atmospheric Research Satellite measurements of the hydroxyl airglow: 1. Validation of technique, J. Geophys. Res., 108, 4662, doi:10.1029/2003JD003454, D21, 2003.

Schwartz, M., Froidevaux, L., Livesey, N., and Read, W.: MLS/Aura Level 2 Ozone (O_3) Mixing Ratio V004, Greenbelt, MD, USA, Goddard Earth Sciences Data and Information Services Center (GES DISC), accessed 13.07.16, doi:10.5067/AURA/MLS/DATA2017, 2015.

Scinocca, J. F., McFarlane, N. A., Lazare, M., Li, J., Plummer, D.: The CCCma third generation AGCM and its extension into the middle atmosphere, Atmos. Chem. Phys., 8, 7055-7074, doi:10.5194/acp-8-7055-2008, 2008.

Shimazaki, T.: Minor Constituents in the Middle Atmosphere, D. Reidel, Norwell, Mass., USA, 444 pp., 1985.

Siskind, D. E., Marsh, D. R., Mlynczak, M. G., Martin-Torres, F. J., and Russell III, J. M.: Decreases in atomic hydrogen over the summer pole: Evidence for dehydration from polar mesospheric clouds?, Geophys. Res. Lett., 35, L13809, doi:10.1029/2008GL033742, 2008.

Siskind D. E., Mlynczak, M. G., Marshall, T., Friedrich, M., Gumbel, J.: Implications of odd oxygen observations by the TIMED/SABER instrument for lower D region ionospheric modeling, J. Atmos. Sol. Terr. Phys., 124, 63–70, doi: 10.1016/j.jastp.2015.01.014, 2015.

Smith, A. K., Marsh, D. R., Mlynczak, M. G., and Mast, J. C.: Temporal variations of atomic oxygen in the upper mesosphere from SABER, J. Geophys. Res., 115, D18309, doi:10.1029/2009JD013434, 2010.

Sobanski, N., Tang, M. J., Thieser, J., Schuster, G., Pöhler, D., Fischer, H., Song, W., Sauvage, C., Williams, J., Fachinger, J., Berkes, F., Hoor, P., Platt, U., Lelieveld, J., and Crowley, J. N.: Chemical and meteorological influences on the lifetime of NO3 at a semi-rural mountain site during PARADE, Atmos. Chem. Phys., 16, 4867-4883, doi:10.5194/acp-16-4867-2016, 2016.

Solomon, S., Rusch, D. W., Gerard, J.-C., Reid, G. C., and Crutzen, P. J.: The effect of particle precipitation events on the neutral and ion chemistry of the middle atmosphere. 2. Odd hydrogen, Planet. Space Sci., 29, 885–892, 1981.

Sonnemann, G., Kremp, C., Ebel, A., and Berger, U.: A three-dimensional dynamic model of minor constituents of the mesosphere, Atmos. Environ., 32, 3157–3172, doi:10.1016/S1352-2310(98)00113-7, 1998.

Sonnemann, G. R., Grygalashvyly, M., Hartogh, P., and Jarchow, C.: Behavior of mesospheric ozone under nearly polar night conditions, Adv. Space Res., 38, 2402–2407, doi:10.1016/j.asr.2006.09.011, ~~2006a~~2006.

Sonnemann, G. R., Hartogh, P., Jarchow, C., Grygalashvyly, M., and Berger, U.: On the winter anomaly of the night-to-day ratio of ozone in the middle to upper mesosphere in middle to high latitudes, Adv. Space Res., 40, 846–854, doi:10.1016/j.asr.2007.01.039, 2007.

Sonnemann, G. R., Hartogh, P., Berger, U., and Grygalashvyly, M.: Hydroxyl layer: trend of number density and intra-annual variability Ann. Geophys., 33, 749–767, doi:10.5194/angeo-33-749-2015, 2015.

Swenson, G. R., and Gardner, C. S.: Analytical models for the responses of the mesospheric OH* and Na layers to atmospheric gravity waves, J. Geophys. Res., 103(D6), 6271–6294, doi:10.1029/97JD02985, 1998.

Solomon, P., Connor, B., Barrett, J., Mooney, T., Lee, A., and Parrish, A.: Measurements of stratospheric ClO over Antarctica in 1996–2000 and implications for ClO dimer chemistry, Geophys. Res. Lett., 29(15), 1708, doi:10.1029/2002GL015232, 2002.

Stedman, D. H., Chameides, W., and Jackson, J. O.: Comparison of experimental and computed values for J(NO_2), Geophys. Res. Lett., 2(1), 22-25, doi:1029/GL002i001p00022, 1975.

Stimpfle, R. M., Wilmouth, D. M., Salawitch, R. J., and Anderson, J. G.: First measurements of ClOOCl in the stratosphere: The coupling of ClOOCl and ClO in the Arctic polar vortex, J. Geophys. Res., 109, D03301, doi:10.1029/2003JD003811, 2004.

Sumińska-Ebersoldt, O., Lehmann, R., Wegner, T., Grooß, J.-U., Hösen, E., Weigel, R., Frey, W., Griessbach, S., Mitev, V., Emde, C., Volk, C. M., Borrmann, S., Rex, M., Stroh, F., and von Hobe, M.: ClOOCl photolysis at high solar zenith angles: analysis of the RECONCILE self-match flight, Atmos. Chem. Phys., 12, 1353-1365, doi:10.5194/acp-12-1353-2012, 2012.

Thomas, R. J.: Atomic hydrogen and atomic oxygen density in the mesosphere region: Global and seasonal variations deduced from Solar Mesosphere Explorer near-infrared emissions, J. Geophys. Res., 95, 16,457–16,476, doi:10.1029/JD095iD10p16457, 1990.

Tulet, P., Grini, A., Griffin, R. J., and Petitcol, S.: ORILAM-SOA: A computationally efficient model for predicting secondary organic aerosols in three-dimensional atmospheric models, J. Geophys. Res., 111, D23208, doi:10.1029/2006JD007152, 2006.

von Hobe, M., Grooß, J.-U., Müller, R., Hrechanyy, S., Winkler, U., and Stroh, F.: A re-evaluation of the ClO/Cl2O2 equilibrium constant based on stratospheric in-situ observations, Atmos. Chem. Phys., 5, 693-702, doi:10.5194/acp-5-693-2005, 2005.

von Hobe, M., Salawitch, R. J., Canty, T., Keller-Rudek, H., Moortgat, G. K., Grooß, J.-U., Müller, R., and Stroh, F.: Understanding the kinetics of the ClO dimer cycle, Atmos. Chem. Phys., 7, 3055-3069, doi:10.5194/acp-7-3055-2007, 2007.

Walcek, C. J., and N. M. Aleksic (1998), A simple but accurate mass conservative, peak preserving, mixing ratio bounded advection algorithm with Fortran code, Atmos. Environm., 32, 3863-3880.

Walcek, C. J. (2000), Minor flux adjustment near mixing ratio extremes for simplified yet highly accurate monotonic calculation of tracer advection, J. Geophys. Res., 105, 9335-9348.

Wang, S., Pickett, H., Livesey, N., and Read, W.: MLS/Aura Level 2 Hydroperoxy (HO_2) Mixing Ratio V004, Greenbelt, MD, USA, Goddard Earth Sciences Data and Information Services Center (GES DISC), accessed 13.07.16, doi:10.5067/AURA/MLS/DATA2013, 2015a.

Wang, S., Livesey, N., and Read, W.: MLS/Aura Level 2 Hydroxyl (OH) Mixing Ratio V004, Greenbelt, MD, USA, Goddard Earth Sciences Data and Information Services Center (GES DISC), accessed 13.07.16, doi:10.5067/AURA/MLS/DATA2018, 2015b.

Webster, C. R., May, R. D., Toumi, R., and Pyle, J. A.: Active nitrogen partitioning and the nighttime formation of N2O5 in the stratosphere: Simultaneous in situ measurements of NO, NO_2, HNO_3, O_3, and N_2O using the BLISS diode laser spectrometer, J. Geophys. Res., 95(D9), 13851–13866 doi: 10.1029/JD095iD09p13851, 1990.

Wetzel, G., Oelhaf, H., Kirner, O., Friedl-Vallon, F., Ruhnke, R., Ebersoldt, A., Kleinert, A., Maucher, G., Nordmeyer, H., and Orphal, J.: Diurnal variations of reactive chlorine and nitrogen oxides observed by MIPAS-B inside the January 2010 Arctic vortex, Atmos. Chem. Phys., 12, 6581-6592, doi:10.5194/acp-12-6581-2012, 2012.

Xu, J., Smith, A. K., Jiang, G., Gao, H., Wei, Y., Mlynczak, M. G. ,and Russell III, J. M.: Strong longitudinal variations in the OH nightglow, Geophys. Res. Lett., 37, L21801, doi:10.1029/2010GL043972, 2010.

Xu, J., Gao, H., Smith, A. K., and Zhu, Y.: Using TIMED/SABER nightglow observations to investigate hydroxyl emission mechanisms in the mesopause region, J. Geophys. Res., 117, D02301, doi:10.1029/2011JD016342, 2012.

Table 1. List of reactions with corresponding reaction rates from Burkholder et al. (2015).

1	$O(^1D)+O_2 \rightarrow O+O_2$	22	$OH+O_3 \rightarrow O_2+HO_2$	43	$NO_2+O_3 \rightarrow NO_3+O_2$
2	$O(^1D)+N_2 \rightarrow O+N_2$	23	$HO_2+O_3 \rightarrow OH+2O_2$	44	$N+OH \rightarrow NO+H$
3	$O(^1D)+O_3 \rightarrow O_2+2O$	24	$H+OH+N_2 \rightarrow H_2O+N_2$	45	$NO+HO_2 \rightarrow NO_2+OH$
4	$O(^1D)+O_3 \rightarrow 2O_2$	25	$OH+H_2 \rightarrow H_2O+H$	46	$H+NO_2 \rightarrow OH+NO$
5	$O(^1D)+N_2O \rightarrow 2NO$	26	$OH+OH \rightarrow H_2O+O$	47	$NO_3+NO \rightarrow 2NO_2$
6	$O(^1D)+N_2O \rightarrow N_2+O_2$	27	$OH+OH+M \rightarrow H_2O_2+M$	48	$N+NO \rightarrow N_2+O$
7	$O(^1D)+H_2O \rightarrow 2OH$	28	$OH+HO_2 \rightarrow H_2O+O_2$	49	$N+NO2 \rightarrow N2O+O$
8	$O(^1D)+H_2 \rightarrow H+OH$	29	$H_2O_2+OH \rightarrow H_2O+HO_2$	50	$O_2+h\nu \rightarrow 2O$
9	$O(^1D)+CH_4 \rightarrow CH_3+OH$	30	$HO_2+HO_2 \rightarrow H_2O_2+O_2$	51	$O_2+h\nu \rightarrow O+O(^1D)$
10	$O(^1D)+CH_4 \rightarrow H_2+CH_2O$	31	$HO_2+HO_2+M \rightarrow H_2O_2+O_2+M$	52	$O_3+h\nu \rightarrow O_2+O$
11	$O+O+M \rightarrow O_2+M$	32	$CH_3+O \rightarrow CH_2O+H$	53	$O_3+h\nu \rightarrow O_2+O(^1D)$
12	$O+O_2+M \rightarrow O_3+M$	33	$OH+CO \rightarrow H+CO_2$	54	$N_2+h\nu \rightarrow 2N$
13	$O+O_3 \rightarrow O_2+O_2$	34	$CH_4+OH \rightarrow CH_3+H_2O$	55	$NO+h\nu \rightarrow N+O$
14	$H+HO_2 \rightarrow 2OH$	35	$CH_3+O_2+M \rightarrow CH_3O_2+M$	56	$NO_2+h\nu \rightarrow NO+O$
15	$H+HO_2 \rightarrow H_2O+O$	36	$O_3+N \rightarrow NO+O_2$	57	$N_2O+h\nu \rightarrow N_2+O(^1D)$
15	$H+HO_2 \rightarrow H_2+O_2$	37	$NO_3+O \rightarrow NO_2+O_2$	58	$N_2O+h\nu \rightarrow N+NO$
17	$OH+O \rightarrow H+O_2$	38	$O+NO+M \rightarrow NO_2+M$	59	$H_2O+h\nu \rightarrow H+OH$
18	$HO_2+O \rightarrow OH+O_2$	39	$NO_2+O \rightarrow NO+O_2$	60	$CH_4+h\nu \rightarrow CH_2+H_2$
19	$H_2O_2+O \rightarrow OH+HO_2$	40	$NO_2+O+M \rightarrow NO_3+M$	61	$H_2O_2+h\nu \rightarrow 2OH$
20	$H+O_2+M \rightarrow HO_2+M$	41	$N+O_2 \rightarrow NO+O$	62	$NO_3+h\nu \rightarrow NO_2+O$
21	$H+O_3 \rightarrow OH+O_2$	42	$NO+O_3 \rightarrow NO_2+O_2$	63	$CO_2+h\nu \rightarrow CO+O$

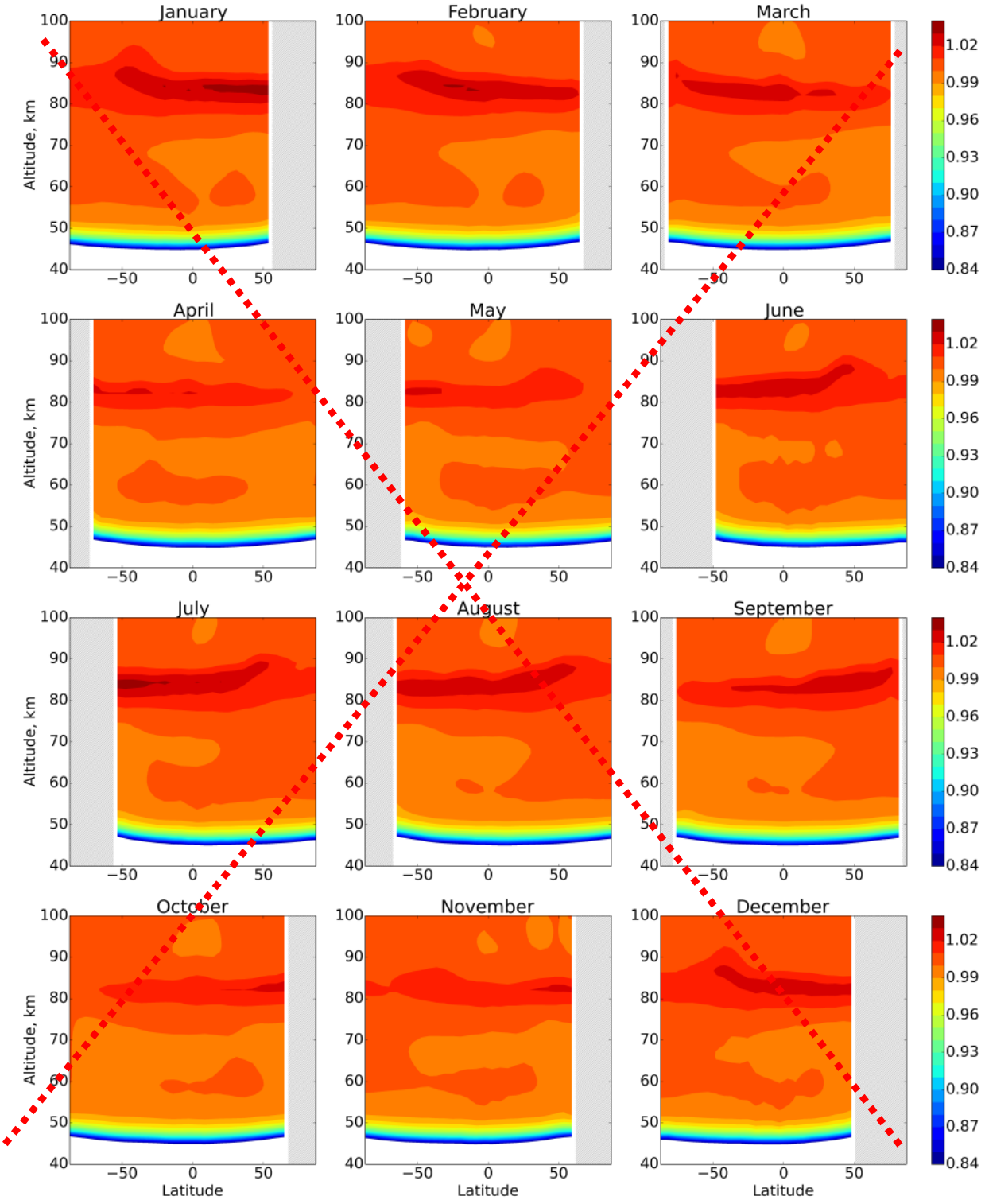

Figure 1. Daytime monthly averaged zonal mean $\langle F \rangle$ distributions.

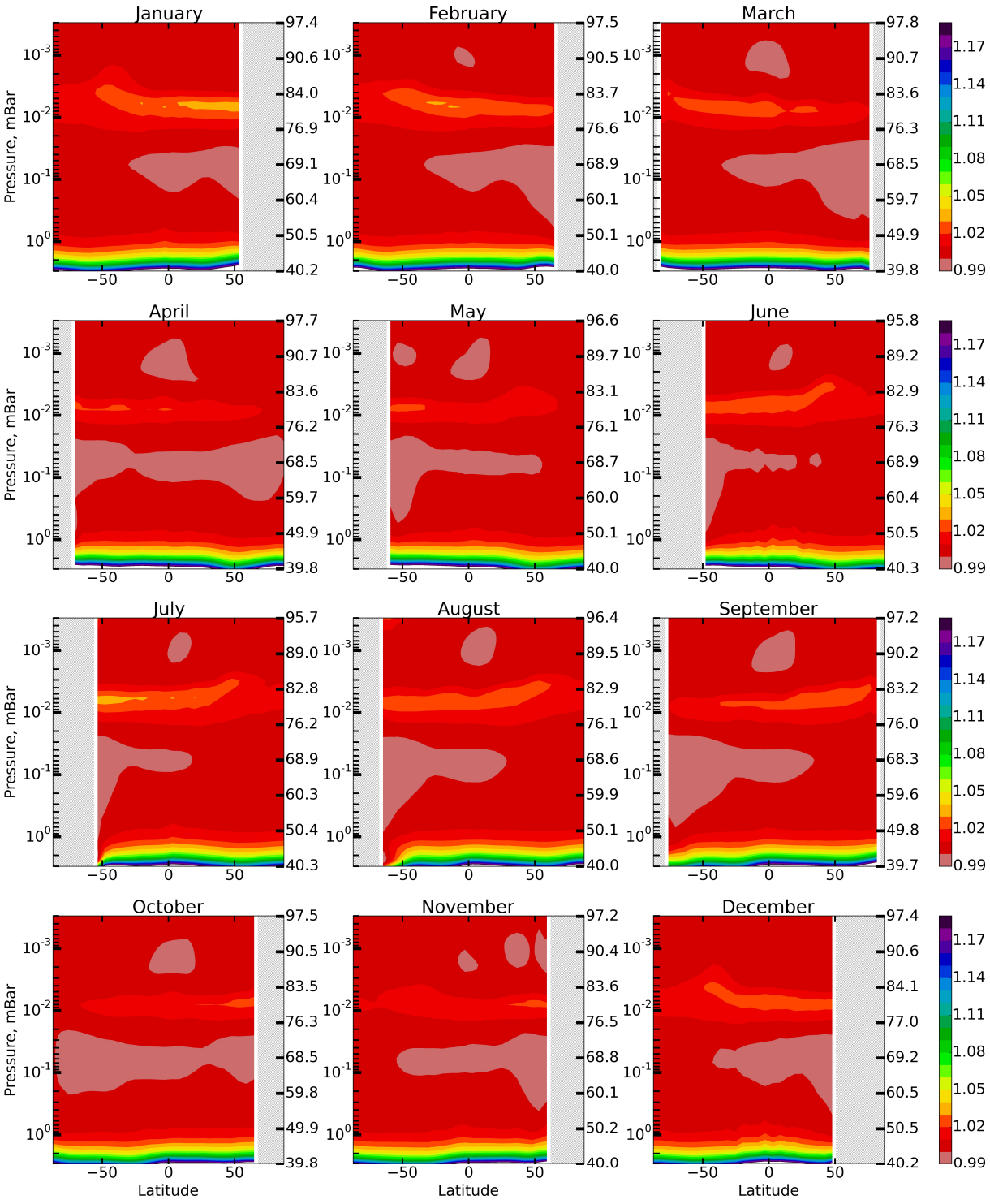

Figure 1. Daytime monthly averaged zonal mean $\langle F \rangle$ F distributions.

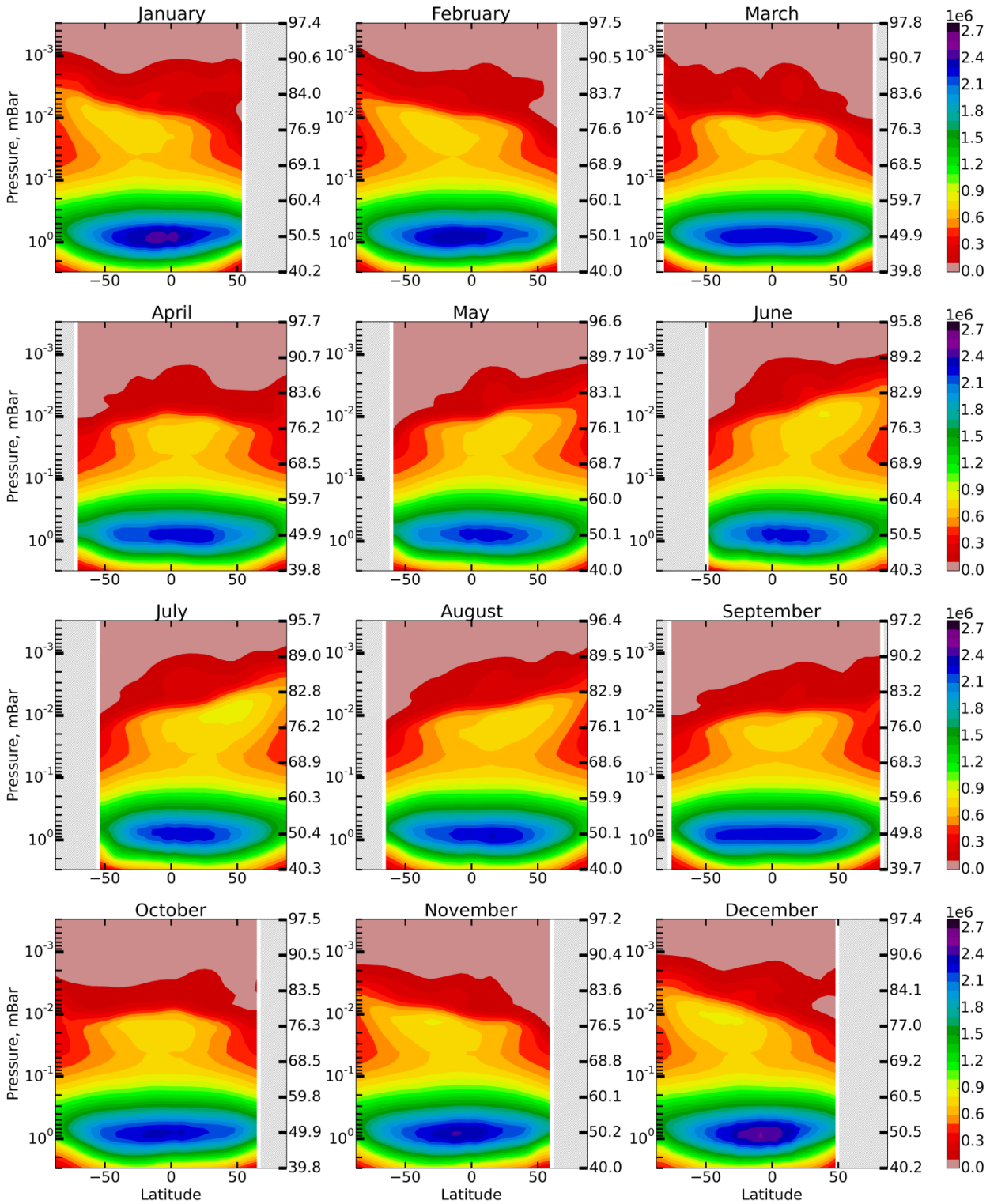

Figure 2. Daytime monthly averaged zonal mean P_{OH} distributions (in $cm^{-3}s^{-1}$).

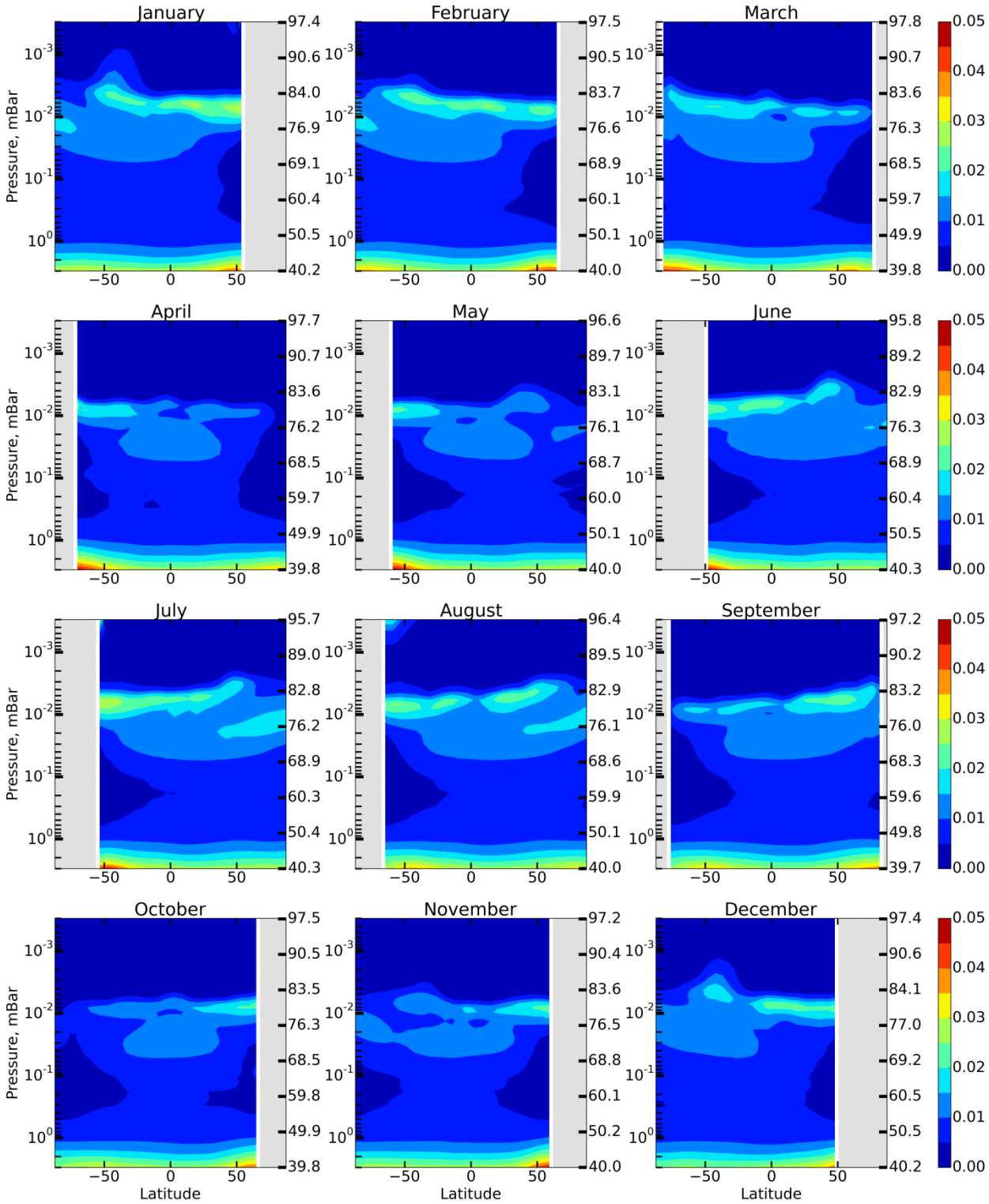

Figure 3. Daytime monthly averaged zonal mean $P_{OH}^{H_2O} / P_{OH}$ distributions.

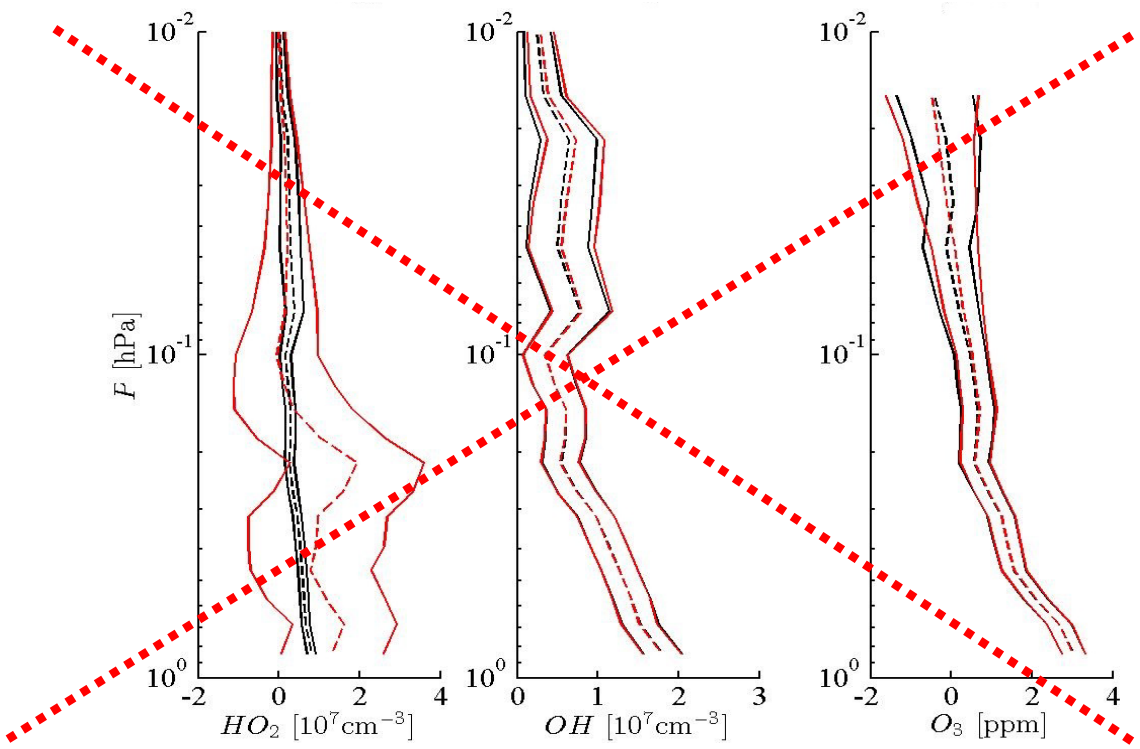

~~Figure 2. Example of OH, HO_2 and O_3 vertical profiles measured (red curves) on 15 January 2005 at 13.07 UT, 38.53^{0}N, 357.33^{0}W and corresponding retrieved profiles (black curves). Solid curves: boundaries of the 65% confident intervals, dashed curves: medians.~~

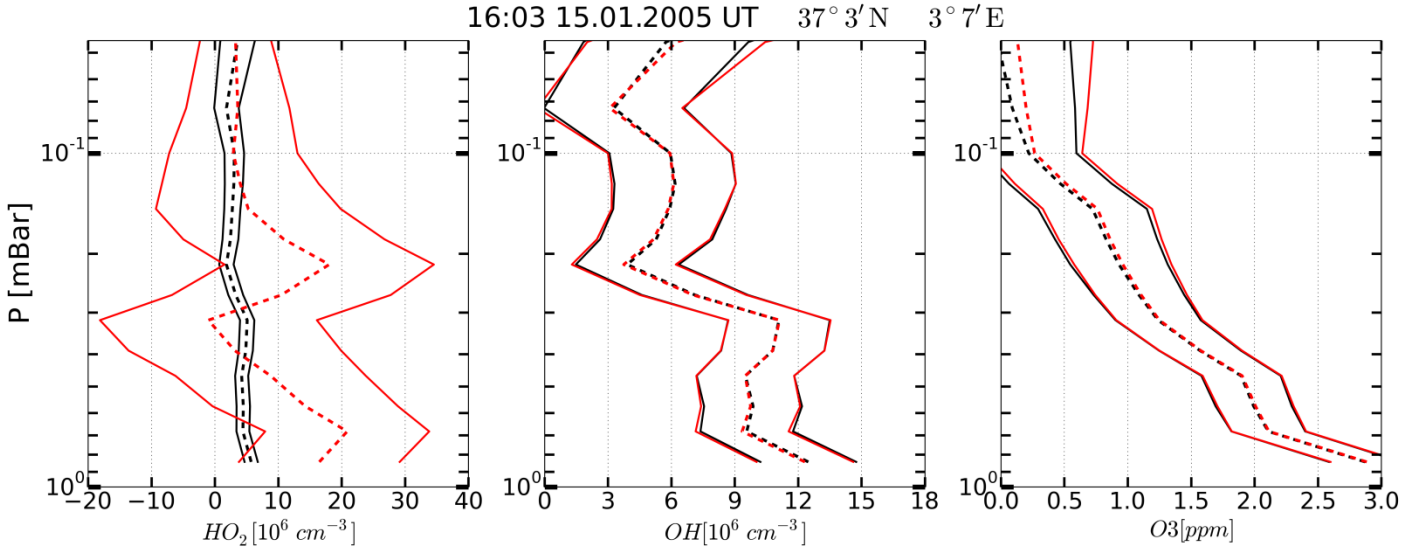

Figure 4. Example of OH, HO_2 and O_3 vertical profiles measured (red curves) on 15 January 2005 at 16.03 UT, 37^{0}3'N, 3^{0}7'E and corresponding retrieved profiles (black curves). Solid curves: boundaries of the 65% confident intervals, dashed curves: medians.

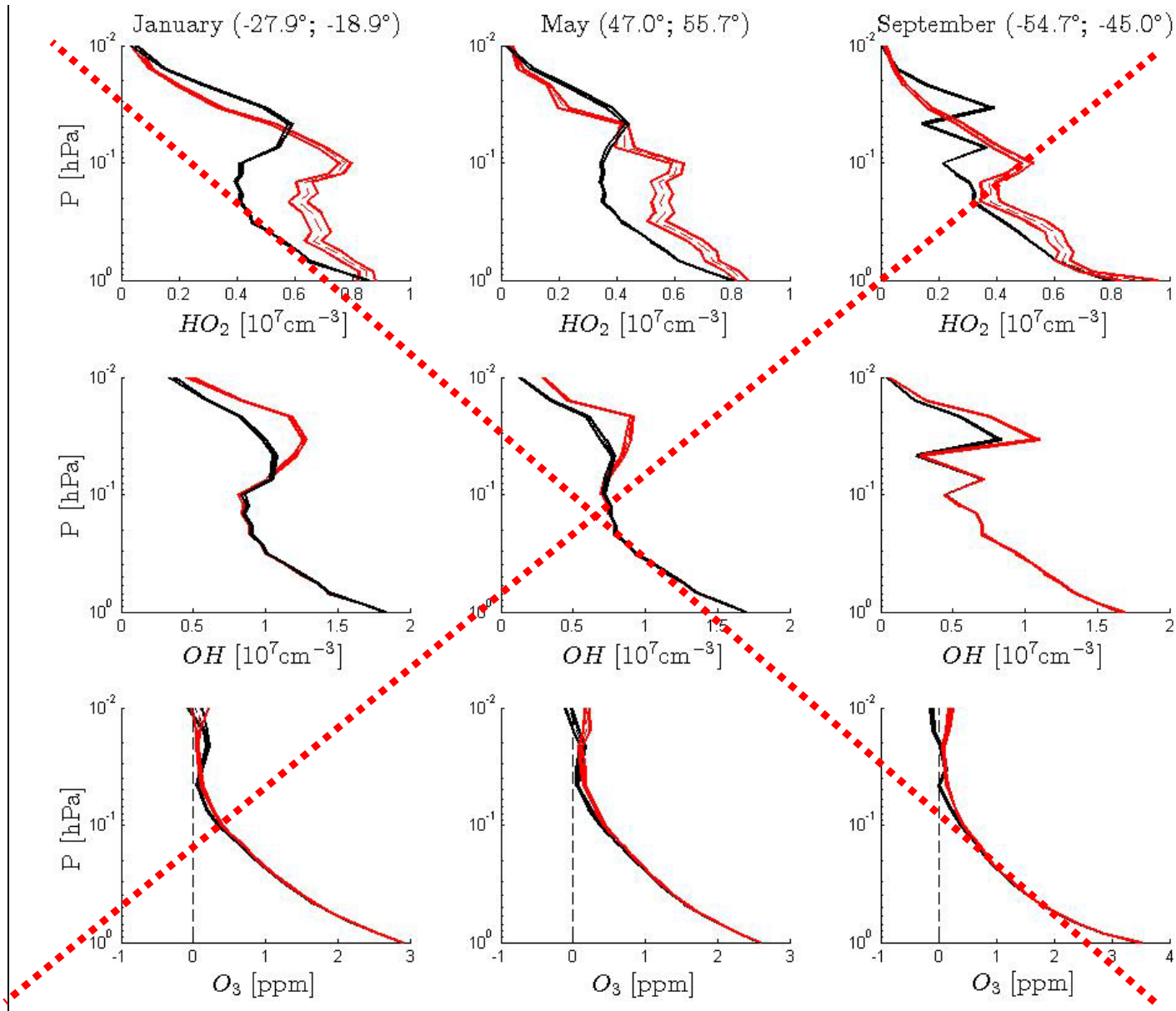

Figure 3. Examples of monthly averaged zonal mean vertical profiles of OH, HO_2 and O_3 measured (red curves) in January, May and March 2005 and corresponding retrieved profiles (black curves). Solid curves: boundaries of the 65% confident intervals, dashed curves: medians.

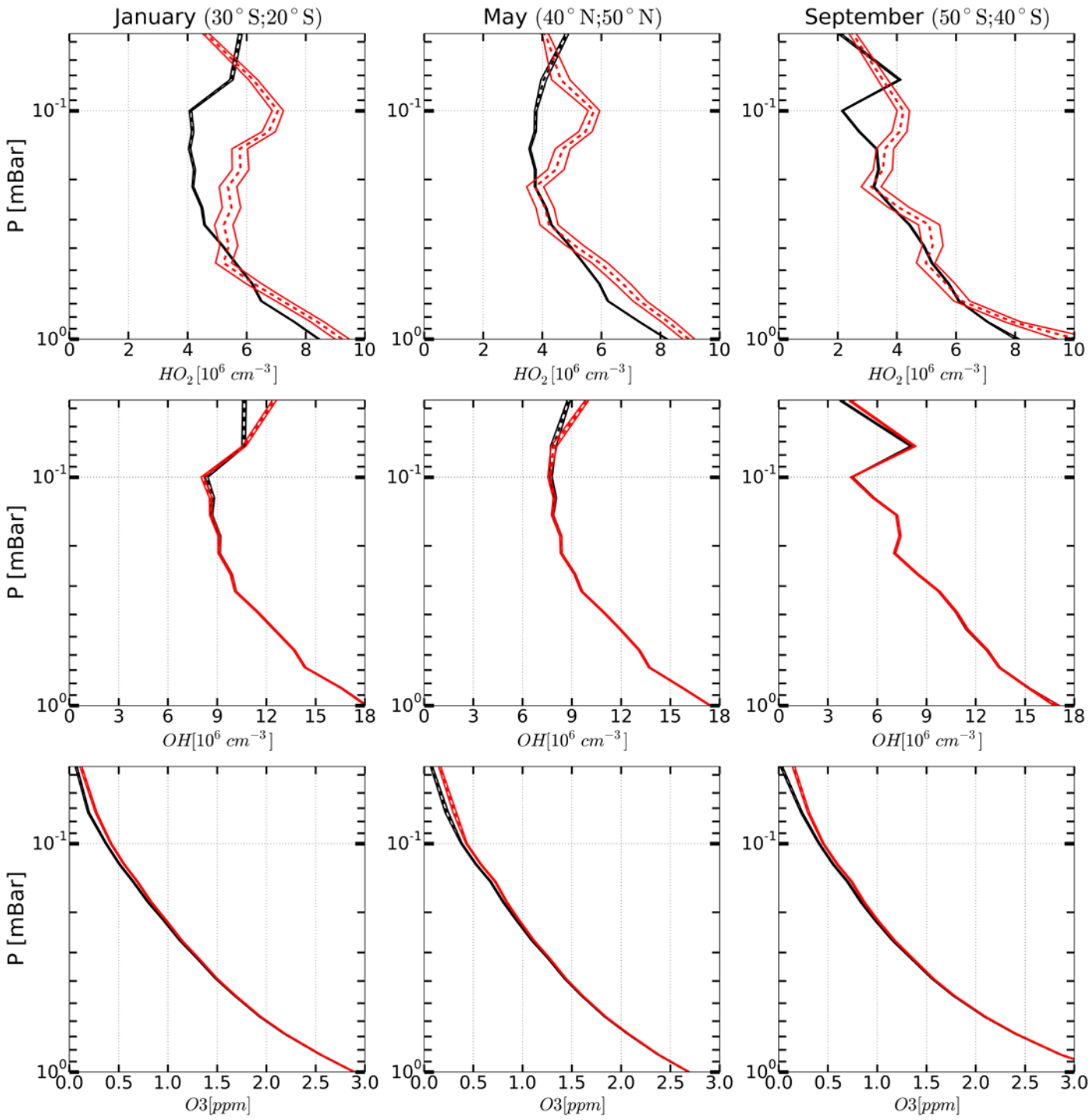

Figure 5. Examples of monthly averaged zonal mean vertical profiles of OH, HO_2 and O_3 measured (red curves) in January, May and March 2005 and corresponding retrieved profiles (black curves). Solid curves: boundaries of the 65% confident intervals, dashed curves: medians.

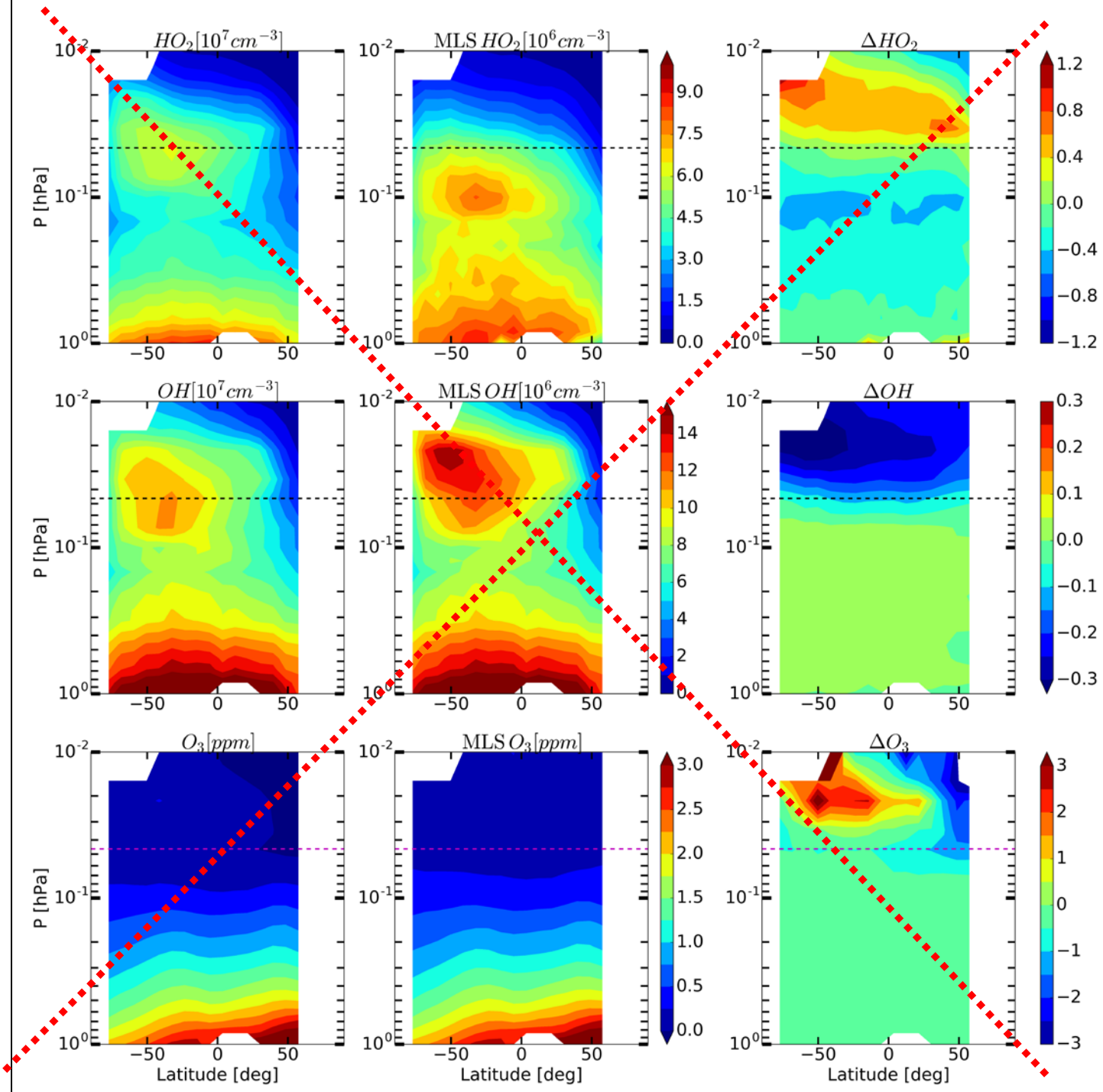

Figure 4. Daytime monthly averaged zonal mean retrieved (left column) and measured (middle column) distributions of HO_2, OH, and O_3 and their relative difference (right column) in January 2005.

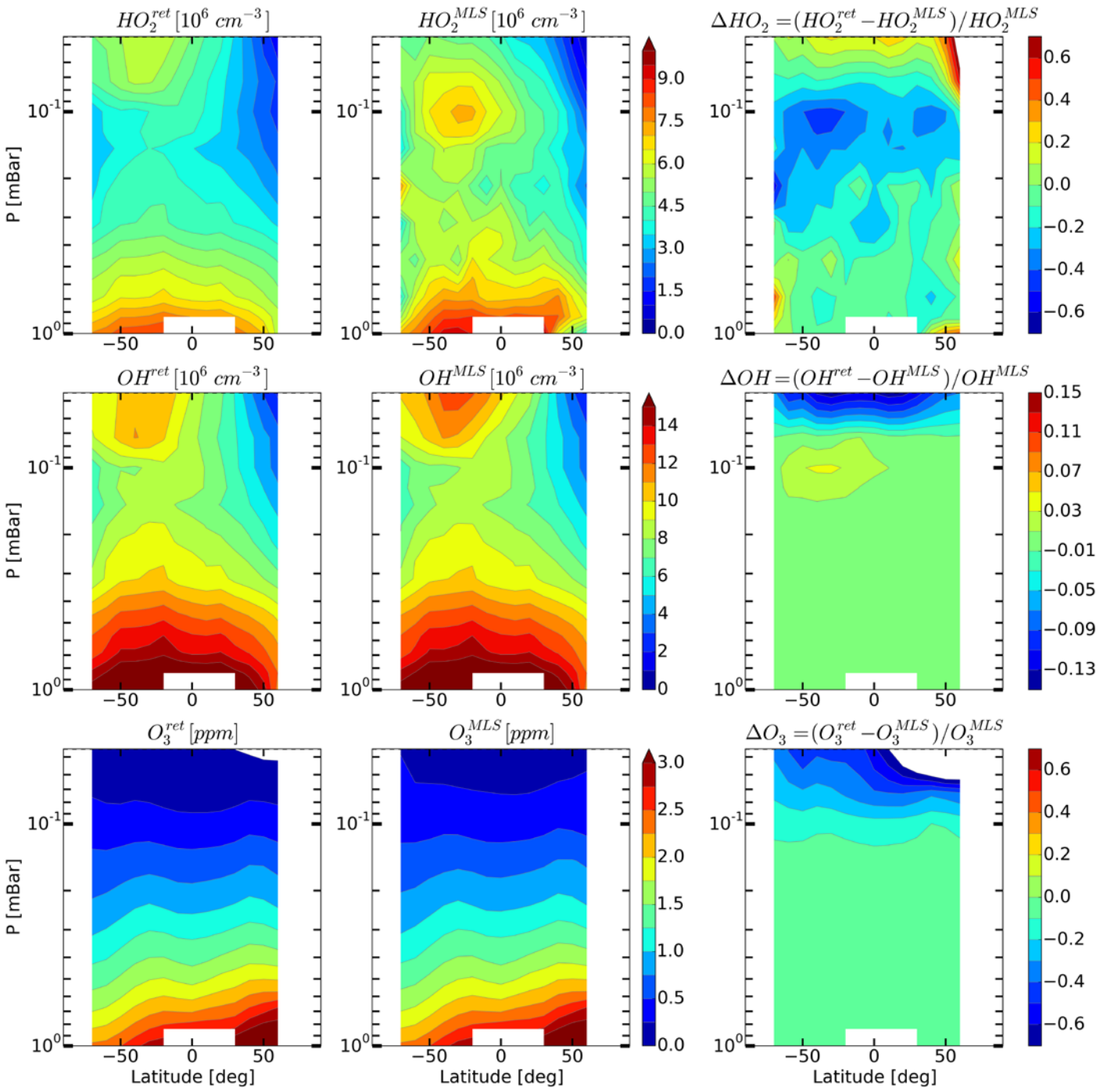

Figure 6. Daytime monthly averaged zonal mean retrieved (left column) and measured (middle column) distributions of HO_2, OH, and O_3 and their relative difference (right column) in January 2005.

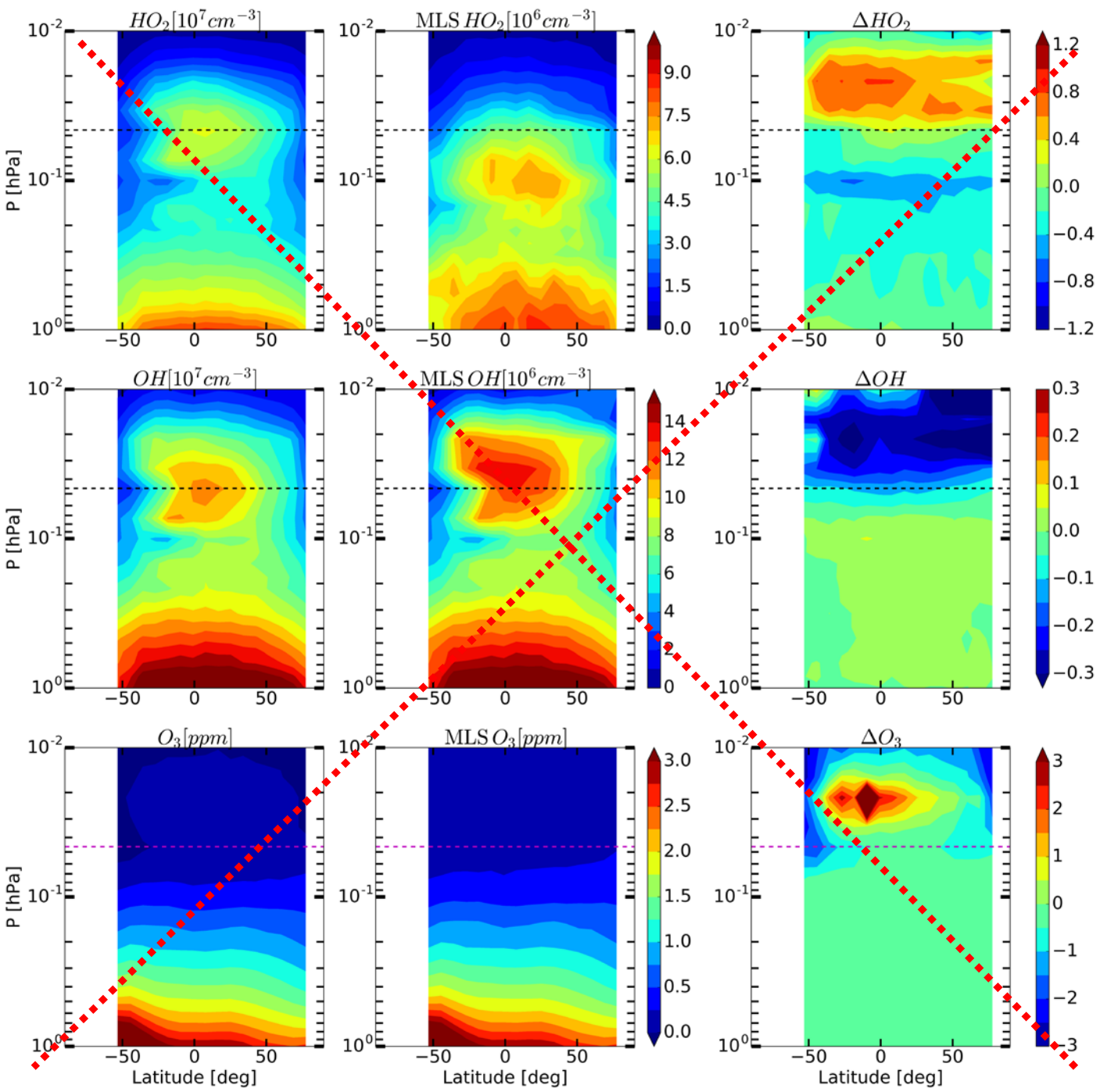

Figure 5. Daytime monthly averaged zonal mean retrieved (left column) and measured (middle column) distributions of HO_2, OH, and O_3 and their relative difference (right column) for May 2005.

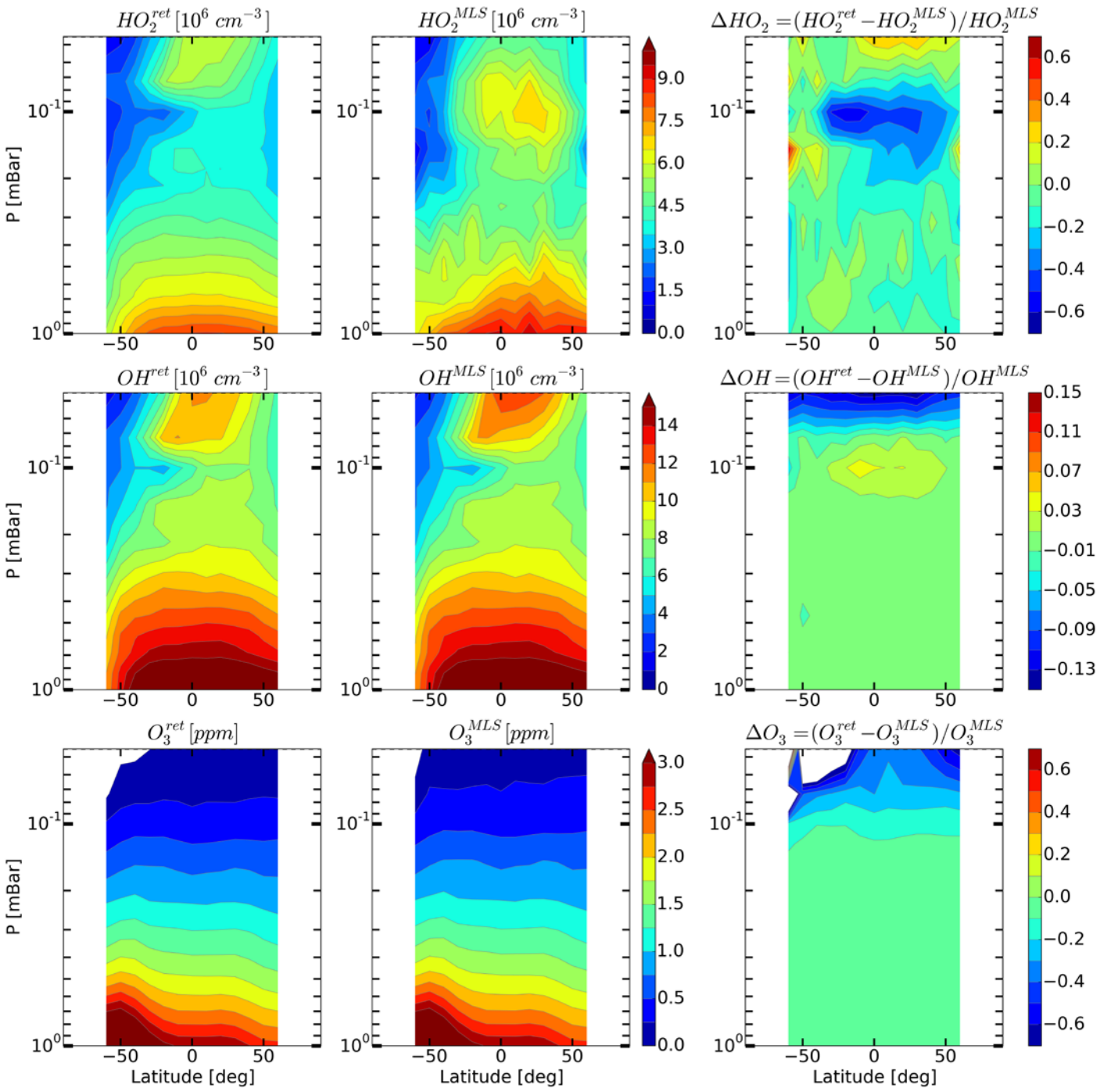

Figure 7. Daytime monthly averaged zonal mean retrieved (left column) and measured (middle column) distributions of HO_2, OH, and O_3 and their relative difference (right column) for May 2005.

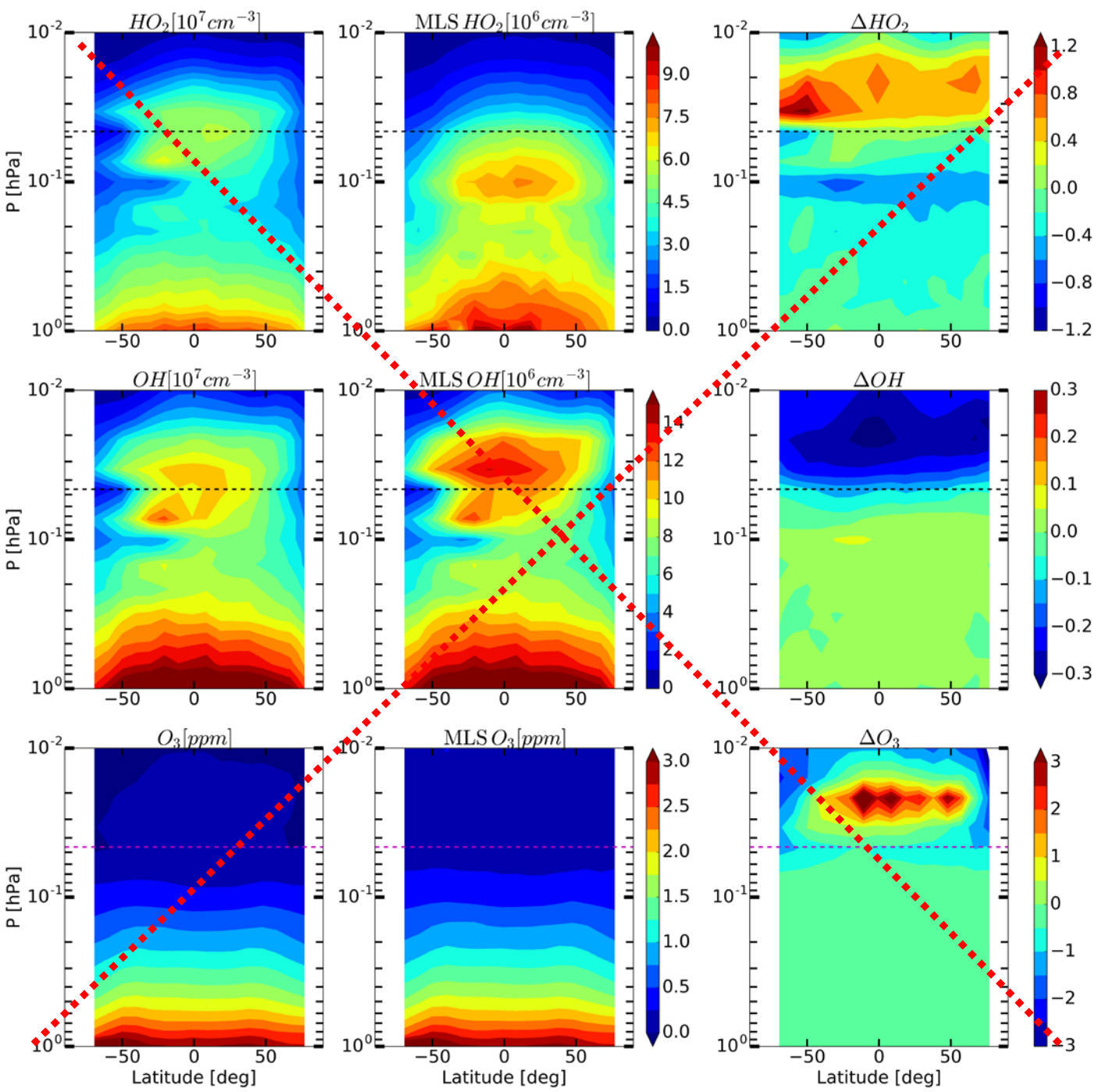

~~Figure 6. Daytime monthly averaged zonal mean retrieved (left column) and measured (middle column) distributions of HO_2, OH, and O_3 and their relative difference (right column) for September 2005.~~

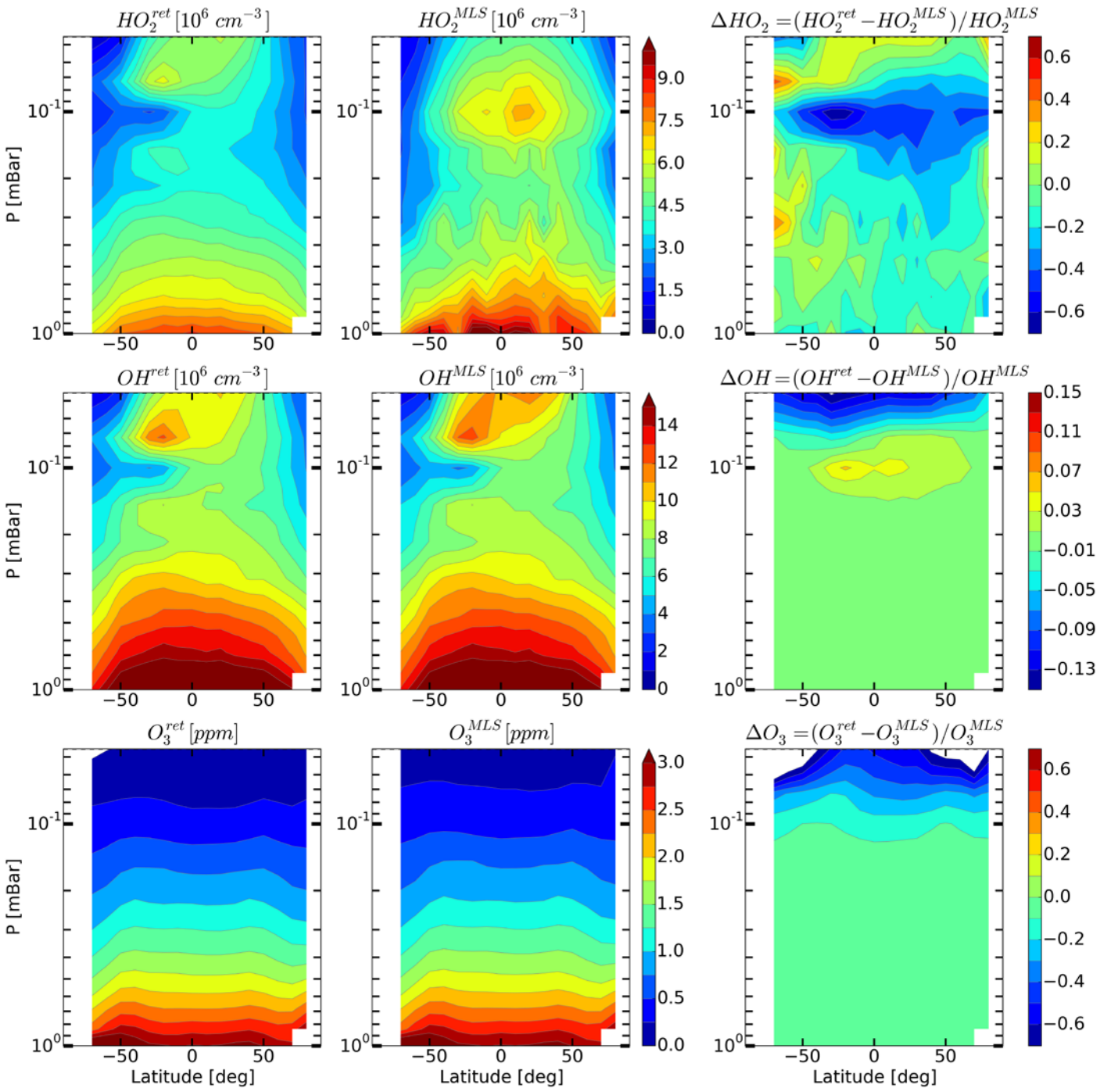

Figure 8. Daytime monthly averaged zonal mean retrieved (left column) and measured (middle column) distributions of HO_2, OH, and O_3 and their relative difference (right column) for September 2005.

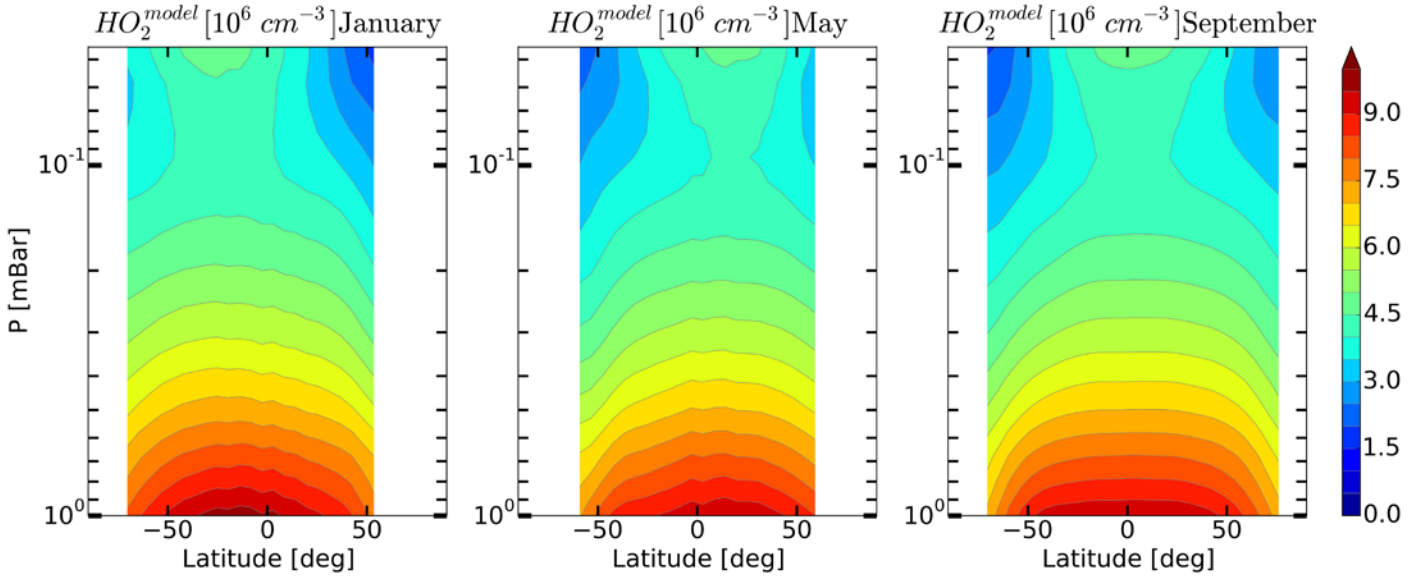

948

949 Figure 9. Daytime monthly averaged zonal mean model distributions of HO_2 for January, May, and

950 September

951

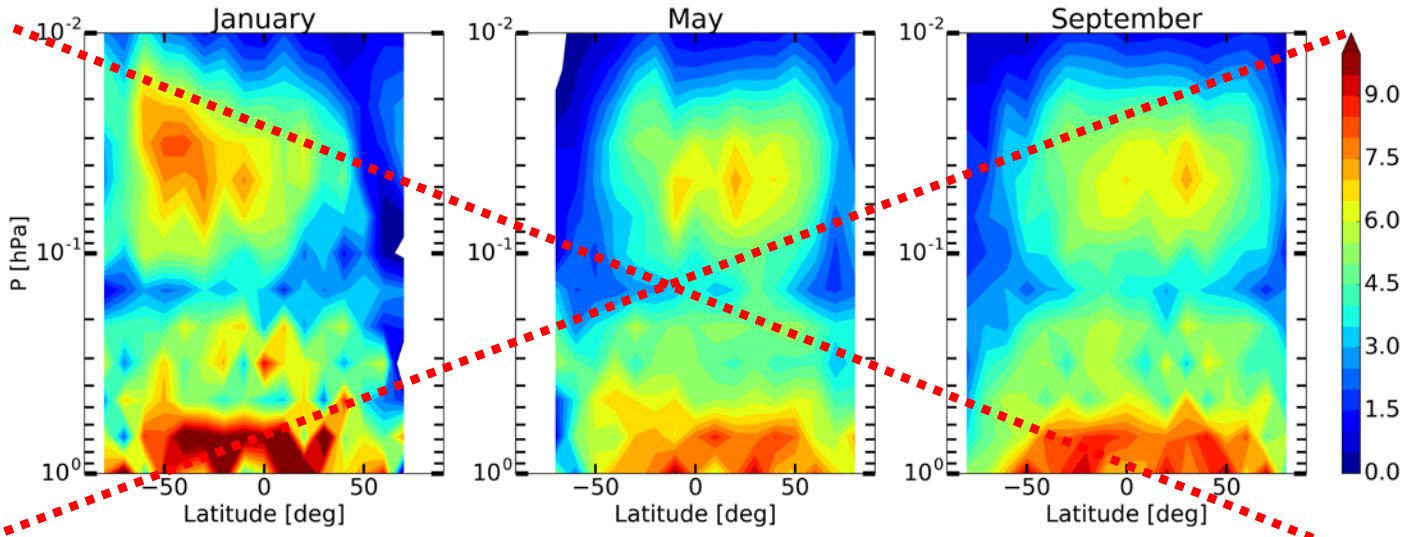

Figure 7. Daytime mean monthly averaged distributions of HO_2 retrieved by Millán et al. (2015) from MLS primary data.

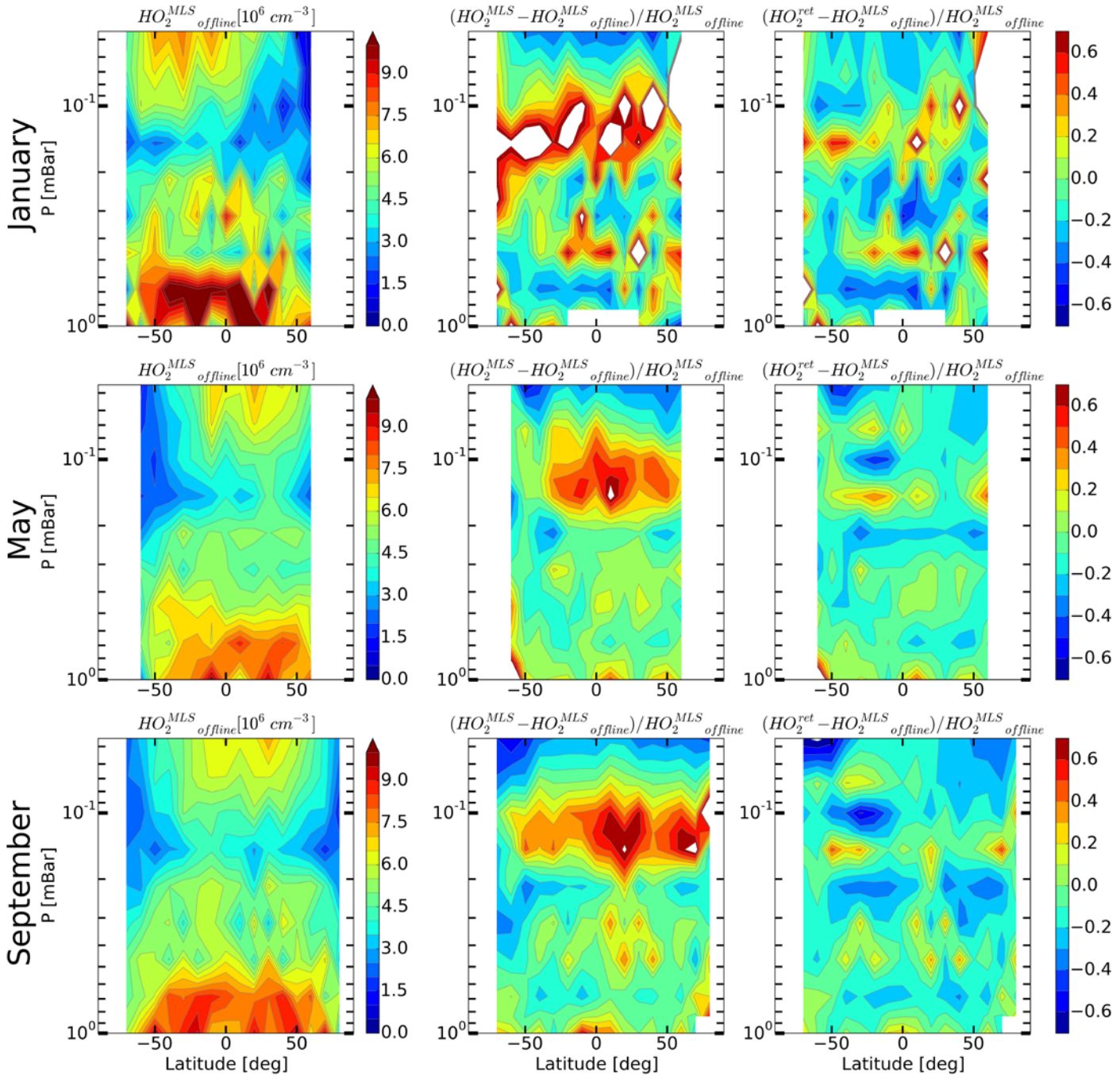

Figure 10. Daytime mean monthly averaged distributions of HO_2 retrieved by Millán et al. (2015) and relative differences $(<HO_2^{MLS}> - <HO_2^{MLS}{}_{offline}>)/<HO_2^{MLS}{}_{offline}>$ and $(<HO_2^{ret}> - <HO_2^{MLS}{}_{offline}>)/<HO_2^{MLS}{}_{offline}>$.